



King's Research Portal

DOI:

[10.1038/s41586-019-0901-4](https://doi.org/10.1038/s41586-019-0901-4)

Document Version

Peer reviewed version

[Link to publication record in King's Research Portal](#)

Citation for published version (APA):

Edwards, T. L., Brandon, M., Durand, G., Edwards, N., Golledge, N. R., Holden, P., Nias, I., Payne, A. J., Ritz, C., & Wernecke, A. (2019). Revisiting Antarctic ice loss due to marine ice-cliff instability. *Nature*, 566, 58-64. <https://doi.org/10.1038/s41586-019-0901-4>

Citing this paper

Please note that where the full-text provided on King's Research Portal is the Author Accepted Manuscript or Post-Print version this may differ from the final Published version. If citing, it is advised that you check and use the publisher's definitive version for pagination, volume/issue, and date of publication details. And where the final published version is provided on the Research Portal, if citing you are again advised to check the publisher's website for any subsequent corrections.

General rights

Copyright and moral rights for the publications made accessible in the Research Portal are retained by the authors and/or other copyright owners and it is a condition of accessing publications that users recognize and abide by the legal requirements associated with these rights.

- Users may download and print one copy of any publication from the Research Portal for the purpose of private study or research.
- You may not further distribute the material or use it for any profit-making activity or commercial gain
- You may freely distribute the URL identifying the publication in the Research Portal

Take down policy

If you believe that this document breaches copyright please contact librarypure@kcl.ac.uk providing details, and we will remove access to the work immediately and investigate your claim.

1 **ARTICLE**

2

3 **Revisiting Antarctic ice loss due to marine**
4 **ice cliff instability**

5

6 Tamsin L. Edwards* [a], Mark Brandon [b], Gael Durand [c], Neil R. Edwards [b], Nicholas
7 R. Golledge [d, e], Philip B. Holden [b], Isabel Nias [f], Antony J. Payne [g], Catherine Ritz
8 [c] and Andreas Wernecke [b].

9 * Corresponding author

10

11 a Department of Geography, King's College London

12 b School of Environment Earth and Ecosystem Sciences, Faculty of Science, Technology, Engineering and
13 Mathematics, Open University, Walton Hall. Milton Keynes, UK

14 c Univ. Grenoble Alpes, CNRS, IRD, IGE, F-38000 Grenoble, France

15 d Antarctic Research Centre, Victoria University of Wellington, Wellington 6140, New Zealand

16 e GNS Science, Avalon, Lower Hutt 5011, New Zealand

17 f Earth System Science Interdisciplinary Center, 5825 University Research Court, Suite 4001, College Park,
18 Maryland 20740-3823, USA

19 g Centre for Polar Observation and Modelling, School of Geographical Sciences, University of Bristol,
20 University Road, Bristol BS8 1SS, UK

23 **Predictions for sea-level rise from Antarctica this century range from zero to over one**
24 **metre. The highest are driven by the controversial ‘marine ice cliff instability’ (MICI)**
25 **hypothesis, where coastal ice cliffs rapidly collapse after ice shelves disintegrate from**
26 **surface and sub-shelf melting caused by global warming. But the MICI mechanism has**
27 **not been observed in the modern era, and it remains unclear whether or not it is**
28 **required to reproduce sea-level variations in the geological past. Here we quantify ice**
29 **sheet modelling uncertainties for the original MICI study and show the probability**
30 **distributions are skewed towards lower values (most likely value is 45 cm under very**
31 **high greenhouse gas concentrations). However, MICI is not required to reproduce sea-**
32 **level changes in the mid-Pliocene, Last Interglacial or 1992-2017, and without it we find**
33 **the projections agree with previous studies (all 95th percentiles are less than 43 cm). We**
34 **therefore find previous interpretations of the MICI projections over-estimate sea-level**
35 **rise this century. The hypothesis is not well constrained: confidence in projections with**
36 **MICI would require a greater diversity of observationally constrained models of ice**
37 **shelf vulnerability and ice cliff collapse.**

38 Projections of the Antarctic contribution to global mean sea-level rise this century from
39 process-based models vary widely¹⁻⁶. In particular, DeConto and Pollard (2016)⁶ (here DP16)
40 introduced a hypothesised ‘marine ice cliff instability’ (MICI) process⁷ resulting in mean
41 values exceeding 1 m by 2100 under some methodological choices. However, the DP16
42 results are sensitive to these choices (Table 1: Mean \pm 1 s.d.; Extended Data Figures 1a and
43 b), and the shapes of the probability distributions are very poorly known (Extended Data
44 Figure 2), leading to extremely wide probability intervals (Table 1). This considerable
45 uncertainty poses challenges for robust and cost-effective coastal flood risk management.

46 The Antarctic contribution to global mean sea-level (GMSL) has two parts: increasing
47 snowfall, which is expected to reduce GMSL by a few centimetres this century, and ice
48 discharge into the ocean, which is very uncertain¹. The latter is determined by outflow of ice
49 across the ‘grounding line’ (the boundary between floating and grounded ice), which can
50 increase due to faster ice flow or inland retreat of the grounding line. Ice discharge can
51 increase if buttressing by ice shelves is reduced by (1) ice shelf thinning, caused by enhanced
52 oceanic melting due to circulation changes⁸ or direct warming, or (2) partial or total ice shelf
53 collapse, caused by widening of surface crevasses by meltwater due to atmospheric
54 warming^{9,10}.

55 Marine parts of the ice sheet, lying on bedrock below sea-level, are potentially
56 vulnerable to two hypothesised positive feedbacks that may have led to past collapse of the
57 West Antarctic ice sheet¹¹. Both are based on physical mechanisms with theoretical

58 foundations, but it is not yet clear the degree to which these could lead to positive feedbacks
59 (i.e. widespread, rapid and sustained ice losses). ‘Marine Ice Sheet Instability’ (MISI)¹² is a
60 self-sustaining retreat of the grounding line in regions where the bedrock slopes downward
61 inland, triggered by ice shelf thinning or collapse. Ice thickness at the grounding line
62 increases (due to the bedrock slope), leading to faster ice flow, causing further retreat.
63 Satellite and modelling evidence suggests MISI is underway in West Antarctica^{13,14,15}, though
64 it is unclear the degree to which the driver of this, warm Circumpolar Deep Water breaching
65 the continental shelf, has been affected by human activities^{1,16,17}. ‘Marine Ice Cliff Instability’
66 (MICI)^{6,7} is a self-sustaining retreat of the ice front in regions where the ice is 100 m or more
67 above the ocean surface¹⁸, triggered by ice shelf collapse. These tall ice cliffs are structurally
68 unstable, and their collapse could leave behind further tall cliffs, resulting in sustained ice
69 losses. Observational evidence for MICI is indirect: an absence of ice cliffs taller than 100 m,
70 and rapid retreat of the front of the Jakobshavn (Greenland) and Crane (Antarctic) glaciers
71 (see Knowledge Gaps and Future Directions).

72 DP16⁶ use an Antarctic ice sheet model with a new parameterisation of MICI⁷,
73 generating a 64-member ensemble by varying three parameters controlling the relationship
74 between ocean temperature and basal melting, ice shelf disintegration, and maximum rate of
75 ice cliff collapse. They make projections to 2500 under three Representative Concentration
76 Pathways (RCPs): RCP2.6, RCP4.5 and RCP8.5, for very low, low-to-medium and very high
77 greenhouse gas concentrations respectively¹. They calibrate these by accepting only ensemble
78 members that reproduce reconstructed Antarctic sea-level contributions in the mid-Pliocene
79 (~3 million years ago) and Last Interglacial (LIG: ~130,000–115,000 years ago) eras, and
80 present results for two methodological choices. The first is the Pliocene calibration, using an
81 interval of 5-15 m or 10-20 m; the latter increases sea-level contributions by up to 40 cm by
82 2100 and 2.5 m by 2500 under RCP8.5 (here “LowPliocene”/“HighPliocene”). The second is
83 an ocean temperature correction of +3°C in West Antarctica to improve simulations of the
84 present ice sheet (“BiasCorrected”/“BiasUncorrected”); this increases sea-level contributions
85 by up to 15 cm this century, but makes little difference by 2500. Results for RCP8.5 at 2100
86 are given in Table 1; the corresponding distributions are shown in Extended Data Figure 2.

87 We use statistical techniques for quantifying uncertainties for computationally
88 expensive computer models to re-examine, and estimate probability distributions for, the
89 DP16 projections. We calibrate with the Pliocene, LIG and satellite (1992-2017) eras and
90 make probabilistic projections with and without MICI, comparing with other probabilistic
91 model projections and a Gaussian interpretation of DP16. Finally, we outline knowledge gaps
92 and suggest future directions.

94 **New projections for Antarctica**

95 We estimate probabilistic projections for the Antarctic contribution to sea-level rise by
96 ‘emulating’ the DP16 ice sheet model (see Methods). This quantifies how a computer
97 model’s outputs vary as a function of its input parameters, to predict outputs for any
98 parameter values, enabling us to generate a far larger ensemble than with the original model
99 and to present results both with and without MICI. For this we assume all parameter values
100 are equally likely within the original ranges, based on discussions with the DP16 authors (R.
101 DeConto, pers. comm.). Estimating probability distributions allows meaningful comparison
102 with other studies, and decision-making using sea-level exceedance probabilities under both
103 MICI and No-MICI scenarios. Our method has two further additions: calibration with both
104 palaeodata and satellite data, re-expressing this in the statistical framework of ‘history
105 matching’ (see Methods), and accounting for ice sheet model error.

106 Reconstructions of past climate change provide important tests of models, particularly
107 when the changes were large and/or warmer than today, but their uncertainties are typically
108 large and often poorly-defined¹⁹; recent observations have smaller signals but far smaller
109 uncertainties. The two provide complementary information, so we use both. We use the
110 LowPliocene (equivalent to a combined range of 5-20 m, because the highest simulation is
111 12.4 m), for two reasons: the large reconstruction uncertainty (values lower than 10 m cannot
112 be ruled out: e.g. a more recent estimate has a maximum of 13 m²⁰), and because the DP16
113 projections are very sensitive to the lower bound of the HighPliocene (Extended Data Figure
114 2a and b). The ‘calibration relationships’ between RCP8.5 sea-level contribution at 2100 and
115 sea-level change for the three past eras are shown in Extended Data Figure 3.

116 To estimate probability distributions we use ‘history matching’ (HM), where
117 implausible model versions are excluded, rather than the more commonly known Bayesian
118 calibration (BC), where model versions are weighted by their agreement with observations
119 using a likelihood function (metric of model success). This is for several reasons. The
120 concept of HM is the same as DP16, which allows us to make a simpler and more transparent
121 comparison. This method effectively estimates what DP16 would have found if they had
122 substantially greater computing resources, calibrated their ensemble with satellite data, and
123 accounted for model error. History matching is also more ‘cautious’ than Bayesian model
124 calibration: if no model versions match the data, they are all excluded, while BC retains all
125 and upweights the ‘least bad’. Finally, we do not know the shape of the crucial Bayesian
126 likelihood function for the Pliocene and LIG: this would require estimates of the palaeodata

127 mean and error distribution, rather than assuming all values within the interval are equally
128 likely. Guessing these might shift (wrong mean) or narrow (wrong distribution) the final
129 probability distributions.

130 Accounting for model error, ‘discrepancy’²¹, widens the calibration intervals of
131 acceptance (Extended Data Figures 3 and 4: from grey shaded boxes to dashed lines) and is
132 necessary to avoid over-confidence^{22,23}: the aim is to account for model structural error and
133 other model uncertainties not sampled in the ensemble. These discrepancy terms are
134 tolerances that reflect how well we expect the ice sheet model to reproduce reality. We
135 specify them using expert judgement, including the judgement that they are greater than
136 reconstruction/observation errors^{4,24} (i.e. we judge that confidence in simulating reality with
137 the ice sheet model is lower than in observing or reconstructing it from measurements).
138 Reconstruction errors are not defined by DP16, so we conservatively use half the palaeodata
139 range to avoid underestimating uncertainty (Pliocene: 5 m; LIG: 2 m). For the satellite period,
140 the sea-level change is (0.756 ± 0.386) cm for 1992-2017²⁵; we conservatively specify the
141 model error as 0.5 cm.

142 We present projections at 2100 in Figure 1 and Table 2. The distributions are skewed:
143 modes are consistently lower than medians and means. The results are not strongly dependent
144 on the Pliocene calibration lower bound, unlike the DP16 ensemble, due to the much larger
145 ensemble size (Extended Data Figure 2c: RCP8.5 at 2100 with MICI). Emulated projections
146 without MICI are much lower than those with MICI, and are consistent with previous
147 projections by Ritz et al. (2015)⁴ (Figure 1b). The results are robust to changes in calibration
148 era and discrepancy (Extended Data Figure 5).

149 Crucially, our results show ice cliff instability is not required to reproduce sea-level
150 changes in these three very different eras: 55% of the MICI and 51% of the No-MICI
151 emulator ensemble members simultaneously pass calibration with the Pliocene, LIG and
152 satellite eras (Extended Data Figure 4: larger emulator blue circles within dashed box). MICI
153 increases the ensemble range to encompass more of the data intervals, but the emulator can
154 identify many more areas of the model’s parameter space that are successful: including many
155 without MICI. MICI is therefore not necessary for realistic simulations of these periods, so
156 this positive feedback hypothesis cannot be confirmed or ruled out with this data and
157 calibration method. In fact, the Pliocene does not rule out any ensemble members, because
158 accounting for model error widens the calibration interval to accept them all (Extended Data
159 Figure 3a).

160 The original DP16 projections have substantial probabilities of net sea-level fall this
161 century, with the RCP8.5 LowPliocene mean ± 1 s.d. envelope including negative values

162 until the 2070s. The emulated projections reflect this (Figure 2), though with lower
163 probability (5th percentile negative until the 2070s). Calibration selects mostly positive sea-
164 level contributions during 1992-2017 (Extended Data Figure 3c), then surface accumulation
165 increases with warming (particularly for RCP8.5) and dominates over ice discharge in many
166 ensemble members during this period.

167 We estimate when the hypothesised MICI feedback would accelerate sea-level rise.
168 Contributions with MICI quickly start to diverge from those without for all RCPs: in the
169 2020s (95th percentiles: Figure 2), resulting from the Antarctic Peninsula (DP16: Figure 4c).
170 Dependence of the Antarctic contribution on RCP with MICI begins mid-century, while
171 emergence of a clear, RCP-dependent signal without MICI begins in the 2060s-2070s.

172 We apply the same emulation and calibration methods to the full DP16 time series
173 (Figure 3a). The RCP8.5 distribution remains very skewed, with the mode at the low end of
174 the range; the same is true of RCP4.5, until the 2340s when the mode jumps to the high end
175 of the distribution (from 1.7 m to 4.6 m) and remains there (as seen for 2500). Virtually all
176 the long-term uncertainty arises from MICI. The No-MICI projections remain narrow over
177 multiple centuries – particularly for RCP8.5, which becomes more narrow – because the sea-
178 level contribution in the DP16 ensemble depends less on the parameters controlling ice shelf
179 vulnerability and basal melting over the long-term than during this century. This suggests the
180 DP16 ensemble either seriously under-samples model uncertainties relevant to long-term
181 change, or the model is structurally deficient because the sensitivity to important parameters
182 diminishes under warming. We therefore consider the post-2100 projections to be less
183 reliable.

184 The projected probabilities of exceeding 1 m sea-level contribution over time are shown
185 in Figure 3b. These show that, for high probabilities of first exceeding 1 m Antarctic
186 contribution to sea-level, the difference in exceedance time between RCP8.5 and RCP4.5
187 greenhouse gas concentration scenarios is generally much greater than between projections
188 with or without MICI under RCP8.5. They also show that RCP2.6, i.e. strong mitigation of
189 greenhouse gas concentrations broadly consistent with the 2015 Paris Agreement, is the only
190 one of these scenarios to ensure a low probability of high sea-level rise.

191

192 **Multi-model comparisons**

193 Figure 4 compares the emulated projections at 2100 under RCP8.5 and RCP2.6 with other
194 studies. We compare only with probabilistic projections²⁻⁵, because these have a clear
195 interpretation, and studies that incorporate at least some process-based modelling (rather than

196 only expert elicitation or extrapolation), because we are interested in physical modelling
197 uncertainties and we expect the Antarctica to be governed by different processes in the future
198 than the past (which is not accounted for in extrapolation).

199 We find the emulated No-MICI results agree well with other studies: 95th percentiles
200 are around 30-40 cm under high scenarios and 10-20 cm under low scenarios, despite the use
201 of very different models and approaches (and some differences in scenario and contribution
202 definitions; see Methods). A recent projection by Golledge et al. (2018)²⁶ incorporating ice-
203 ocean-atmosphere feedbacks is also consistent (14 cm under RCP8.5. compared with DP16-
204 based mode of 15 cm; emergence of signal from mid-century). The No-MICI projections for
205 RCP4.5 are very similar to the IPCC (2013) assessment for 2100 relative to 1986–2005¹
206 (Emulated DP16: 5 [–1, 15] cm median and 66% probability interval; IPCC: 5 [–5, 15] cm
207 median and 66% or greater probability). The IPCC (2013) estimates for Antarctic ice
208 discharge do not depend on greenhouse gas scenario, so the projections for RCP2.6 are
209 slightly lower than the IPCC (Emulated DP16: –1 [–7, 7] cm, IPCC: 6 [–4, 16] cm) and
210 higher for RCP8.5 (Emulated DP16: 21 [13, 31] cm, IPCC: 4 [–8, 14] cm).

211 Le Bars et al. (2017)²⁷ make probabilistic interpretations of DP16 for assessing high-
212 end total GMSL by taking the HighPliocene BiasCorrected mean and standard deviation and
213 assuming the distribution is Gaussian. This gives probabilities of exceeding 0.5 m and 1 m
214 Antarctic contribution by 2100 under RCP8.5 of 96% and 65%, respectively. We argue this
215 interpretation is not justifiable, as the original DP16 distributions are skewed (Extended Data
216 Figure 2) and the HighPliocene constraint is not robust (discussed above). Using minimal
217 assumptions about the distribution shape instead would mean probability intervals were very
218 poorly constrained (Table 1). Our estimates of the distribution shape give lower exceedance
219 probabilities: 71% and 36%, respectively (Table 2); We conclude that, although significant
220 sea-level rise is possible under the probability distributions estimated from DP16, Le Bars et
221 al. (2017) systematically overestimate the probability of high sea-level contribution from
222 Antarctica this century.

223 Only Ritz et al. (2015)⁴ have made probabilistic projections beyond 2100. At 2200, the
224 emulated No-MICI projections under RCP8.5 are an order of magnitude higher than Ritz et
225 al. (2015) projections under the medium-high A1B scenario (Figure 3a; emulated median and
226 90% probability interval: 4.0 [3.7, 4.2] m; Ritz et al. (2015): 0.41 [0.04, 0.72] m) and more
227 than double the projections by Golledge et al. (2015)²⁸ for RCP8.5 (0.88 m and 1.52 m at
228 2200 for two model versions). Beyond 2200, the DP16-derived projections under RCP8.5
229 become increasingly inconsistent with Golledge et al. (2015) (Figure 3a). The 2.5th percentile
230 at 2500 without MICI is higher than the latter’s projections at 2500 even under a doubling of

231 RCP8.5 temperature changes. This is particularly surprising, given DP16 greenhouse gas
232 concentrations are capped from the year 2175. However, the RCP4.5 and RCP2.6 No-MICI
233 projections are consistent: the Golledge et al. (2015) ranges fall within the 90% probability
234 intervals.

235 This suggests the DP16 model may be over-sensitive to very large atmospheric
236 temperature changes, even without MICI: i.e. the response is not self-limiting, due to
237 widespread ice shelf sensitivity to warming and/or a lack of local factors mitigating MISI
238 (e.g. bedrock topography, basal traction and sliding, theoretical constraints on ice stresses at
239 the grounding line, and predicted climatic triggers), in contrast to findings from a diversity of
240 other ice sheet and ice shelf models^{4,9,14,15,28,29}.

241

242 **Knowledge gaps and future directions**

243 Our analysis has two aims: to make best estimates of the probability distributions implied by
244 the DP16 study and satellite record, and to evaluate ways in which the original study could be
245 built upon to improve confidence in Antarctic projections. Altering the DP16 climate or ice
246 sheet models, and extending the ensemble parameter ranges, are beyond the scope of this
247 study. For example, we could test the effect of reducing the range of the ice cliff collapse
248 parameter VCLIF (Extended Data Figure 5), but not increasing it. These estimates therefore
249 incorporate many of the limitations of DP16, and should be seen as a first step towards a full
250 assessment of Antarctic sea-level uncertainty.

251 We made pragmatic, simple choices, such as using the same palaeodata intervals as
252 DP16 and uniform distributions for the parameters. Future work should explore alternatives:
253 sampling of the parameter space, palaeodata reconstructions with well-defined uncertainty
254 estimates, spatio-temporal patterns from satellite data, and Bayesian calibration. We are
255 confident that the tails of the sea-level distributions (essential to decision-making) have not
256 been truncated too much by the calibration, as we use a 99.7% probability interval for the
257 satellite data (see Methods) and the palaeodata have very little influence (Extended Data
258 Figure 5). Nevertheless we present projections only to the 95th percentile, to reflect our
259 judgement about the precision of these estimates. Most importantly, presence or absence of
260 MICI is by far the largest uncertainty in sea-level rise this century that could be quantified in
261 this study.

262 Although the maximum height of ice cliffs is founded in theory and indirectly
263 supported by observations and geological evidence^{18,30}, very little is known about whether
264 initial cliff collapse would lead to a positive feedback (i.e. MICI), how this would vary in

265 different locations, the consequent rate of ice wastage, and how long it would last. MICI
266 might be mitigated by cool, fresh meltwater entering the ocean, buttressing by ice mélange,
267 or changes in relative sea-level from gravitational and solid earth effects. Greenland's
268 Helheim and Jakobshavn glaciers have high rates of ice wastage, but this is dominated by
269 their fast flow, not grounding line retreat. Reducing the maximum ice wastage value by 20%
270 to 4 km/a reduces the RCP8.5 projected median by 14% and the 95th percentile by 17%
271 (Extended Data Figure 5), and higher maximum values (which it is not possible to explore in
272 this study) would likely have the opposite effect. The parameterisation of ice loss by MICI in
273 DP16 is very simple, and the low resolution of the model might also over-estimate the
274 occurrence of tall cliffs. A diversity of model parameterisations is therefore needed.

275 Triggers are also poorly understood. DP16 predict early and widespread surface melting
276 (DP16: Extended Data Figure 4) and ice shelf collapse, due to high atmospheric warming,
277 high sensitivity of melting/collapse to warming, or both. This is in contrast with studies using
278 process-based models, which predict up to 5-6 times less surface melting around the
279 Peninsula and 3-8 times less on the West Antarctic Abbot ice shelf by 2100 under RCP8.5¹⁰,
280 and that only shelves along the Peninsula are vulnerable this century under SRES A1B⁹ and
281 RCP8.5¹⁰. Observational evidence of ice shelf melting has highlighted both amplifying and
282 mitigating processes³¹⁻³³, and atmosphere and ocean models have limitations such as present
283 day biases and missing processes, so further process studies and monitoring are required. The
284 DP16 model shows low sensitivity to ocean melting (DP16 Figure 6) and apparently
285 unconstrained response to atmospheric warming (Figure 3a), in contrast with other
286 models^{4,9,14,15,28,29,34}. Again, a greater diversity of models is needed, along with standardised
287 extension of greenhouse gas concentration scenarios, in order to estimate ice sheet stability
288 on multi-centennial timescales. For the Pliocene, DP16 apply a 2°C ocean warming but
289 Golledge et al. (2017)³⁵ estimate this was 3°C, so the contribution to sea-level rise may be
290 under-estimated.

291 Using palaeo-reconstructions to calibrate models requires robust quantification of their
292 uncertainties. History matching calibrations typically use a mean \pm 3 s.d. interval, which for
293 continuous and unimodal distributions corresponds to 95% or greater probability³⁶ for
294 calibration with one observation. For the Pliocene, total GMSL change reconstructed by
295 Miller et al. (2012)³⁷ implies an Antarctic contribution of approximately 4-24 m (95% range),
296 Gasson et al. (2016)²⁰ estimated an Antarctic contribution of -1 to 13 m (with less confidence
297 in the lower bound), Golledge et al. (2017)³⁵ estimated an Antarctic contribution in the early
298 Pliocene of 3-14.2 m (95% range) – all equivalent to, or wider than, the interval used here
299 (i.e. no constraint) – while Raymo et al. (2018)³⁸ argue that Pliocene GMSL is effectively

300 unknown. For the LIG, we have assumed the DP16 range (3.5-7.4 m) is sufficiently broad,
301 but the GMSL estimate by Kopp et al. (2013)³⁹ implies a 90% interval for Antarctica of
302 around 1.6-7.5 m, while the 80% probability interval implied by Dusterhus et al. (2016)⁴⁰
303 (1.3-13.3 m) would virtually eliminate the LIG as a constraint. Long-term deformations in the
304 earth's surface have also recently been estimated to potentially increase estimates of total
305 GMSL at the LIG by up to several metres⁴¹. In fact, emulated projections calibrated only with
306 the satellite period are virtually identical to those calibrated with all three eras (Extended
307 Data Figure 5), indicating that these evaluations with palaeodata have little impact. Using
308 Bayesian calibration (weighting ensemble members by their difference with the data) might
309 yield a stronger constraint, but this would require estimates of mean values and error
310 distributions (e.g. Gaussian).

311 The DP16 ensemble design is not optimal: it includes large gaps and effectively
312 duplicated simulations, and under-samples model uncertainties. Failing to incorporate model
313 error in the calibration also means their projections are likely too narrow and over-confident,
314 a problem amplified by sensitivity to the Pliocene lower bound. Ensemble designs should be
315 space-filling^{4,42} and test which uncertainties are most important to sample (e.g. 'pre-
316 calibration'^{43,44}); emulation allows efficient ensemble design and sensitivity analysis.
317 Statistically-meaningful calibrations (such as history matching and Bayesian updating, with
318 model discrepancy) improves interpretation of the data constraints and robustness and
319 interpretation of the resulting projections.

320 Currently there are few probabilistic Antarctic model projections, and they assess
321 different uncertainties in different ways. We propose a new vision of a 'grand ensemble'
322 designed across multiple diverse ice sheet models simultaneously, systematically sampling
323 parameters, structures, boundary conditions and initial conditions³⁴. Co-ordinated design
324 would allow multi-model emulation, a statistically rigorous method of interpreting and
325 combining different model projections, to estimate probability distributions that account for
326 multiple model structural uncertainties. The Ice Sheet Model Intercomparison Project
327 (ISMIP6) is bringing together an international consortium of ice sheet modellers to make
328 projections for the Greenland and Antarctic ice sheets⁴⁵; this presents an ideal opportunity to
329 design such a framework.

330

- 332 1. IPCC. *Working Group I Contribution to the IPCC Fifth Assessment Report*
333 *Climate Change 2013: The Physical Science Basis*. (Cambridge University
334 Press, 2013).
- 335 2. Little, C. M., Oppenheimer, M. & Urban, N. M. Upper bounds on twenty-first-
336 century Antarctic ice loss assessed using a probabilistic framework. *Nature*
337 *Climate Change* 3, 1–6 (2013).
- 338 3. Levermann, A. *et al.* Projecting Antarctic ice discharge using response functions
339 from SeaRISE ice-sheet models. *Earth Syst. Dynam.* 5, 271–293 (2014).
- 340 4. Ritz, C. *et al.* Potential sea-level rise from Antarctic ice-sheet instability
341 constrained by observations. *Nature* 528, 115–118 (2015).
- 342 5. Ruckert, K. L. *et al.* Assessing the Impact of Retreat Mechanisms in a Simple
343 Antarctic Ice Sheet Model Using Bayesian Calibration. *PLOS ONE* 12,
344 e0170052 (2016).
- 345 6. DeConto, R. M. & Pollard, D. Contribution of Antarctica to past and future sea-
346 level rise. *Nature* 531, 591–597 (2016).
- 347 7. Pollard, D., DeConto, R. M. & Alley, R. B. Potential Antarctic Ice Sheet retreat
348 driven by hydrofracturing and ice cliff failure. *Earth and Planetary Science*
349 *Letters* 412, 112–121 (2015).
- 350 8. Hellmer, H. H., Kauker, F., Timmermann, R., Determann, J. & Rae, J. Twenty-
351 first-century warming of a large Antarctic ice-shelf cavity by a redirected coastal
352 current. *Nature* 485, 225–228 (2012).
- 353 9. Kuipers Munneke, P., Ligtenberg, S. R. M., Van den Broeke, M. R. & Vaughan,
354 D. G. Firm air depletion as a precursor of Antarctic ice-shelf collapse. *Journal of*
355 *Glaciology* 60, 205–214 (2014).
- 356 10. Trusel, L.D. *et al.* Divergent trajectories of Antarctic surface melt under two
357 twenty-first-century climate scenarios. *Nature Geoscience*, 8(12), pp.927–932
358 (2015).
- 359 11. Vaughan, D. G. West Antarctic Ice Sheet collapse – the fall and rise of a
360 paradigm. *Climatic Change* 91, 65–79 (2008).
- 361 12. Schoof, C. Ice sheet grounding line dynamics: Steady states, stability, and
362 hysteresis. *Journal of Geophysical Research* 112, F03S28 (2007).
- 363 13. Rignot, E., Mouginot, J., Morlighem, M., Seroussi, H. & Scheuchl, B.
364 Widespread, rapid grounding line retreat of Pine Island, Thwaites, Smith, and
365 Kohler glaciers, West Antarctica, from 1992 to 2011. *Geophysical Research*
366 *Letters* 41, 3502–3509 (2014).
- 367 14. Favier, L. *et al.* Retreat of Pine Island Glacier controlled by marine ice-sheet
368 instability. *Nature Climate Change* 5, 117–121 (2014).
- 369 15. Joughin, I., Smith, B. E. & Medley, B. Marine Ice Sheet Collapse Potentially
370 Under Way for the Thwaites Glacier Basin, West Antarctica. *Science* 344, 735–
371 738 (2014).
- 372 16. Waugh, D. W., Primeau, F., DeVries, T. & Holzer, M. Recent Changes in the
373 Ventilation of the Southern Oceans. *Science* 339, 568–570 (2013).
- 374 17. Previdi, M. & Polvani, L. M. Climate system response to stratospheric ozone
375 depletion and recovery. *Q J Roy Meteor Soc* 140, 2401–2419 (2014).
- 376 18. Bassis, J. N. & Walker, C. C. Upper and lower limits on the stability of calving
377 glaciers from the yield strength envelope of ice. *Proceedings of the Royal Society*
378 *A: Mathematical, Physical and Engineering Sciences* 468, 913–931 (2012).
- 379 19. Sweeney, J., Salter-Townshend, M., Edwards, T., Buck, C. E. & Parnell, A. C.
380 Statistical Challenges in Estimating Past Climate Changes. *WIREs*
381 *Computational Statistics*, 10 (5), e1437 (2018).

- 382 <https://doi.org/10.1002/wics.1437>
- 383 20. Gasson, E., DeConto, R. M. & Pollard, D. Modeling the oxygen isotope
384 composition of the Antarctic ice sheet and its significance to Pliocene sea-level.
385 *Geology* 44, 827–830 (2016).
- 386 21. Williamson, D., Blaker, A., Hampton, C. & Salter, J. Identifying and removing
387 structural biases in climate models with history matching. *Climate Dynamics* 45,
388 1299–1324 (2014).
- 389 22. McNeall, D. *et al.* The impact of structural error on parameter constraint in a
390 climate model. *Earth Syst. Dynam.* 7, 917–935 (2016).
- 391 23. Williamson, D., Blaker, A. T. & Sinha, B. Tuning without over-tuning:
392 parametric uncertainty quantification for the NEMO ocean model. *Geosci. Model*
393 *Dev.* 10, 1789–1816 (2017). doi:10.5194/gmd-2016-185-AC3
- 394 24. Gladstone, R. M. *et al.* Calibrated prediction of Pine Island Glacier retreat during
395 the 21st and 22nd centuries with a coupled flowline model. *Earth and Planetary*
396 *Science Letters* 333-334, 191–199 (2012).
- 397 25. Shepherd, A. *et al.* Mass balance of the Antarctic Ice Sheet from 1992 to 2017.
398 *Nature* 558, 219–222 (2018).
- 399 26. Golledge, N., E. D. Keller, N. Gomez, K. A. Naughten, J. Bernales, L. D. Trusel,
400 and T. L. Edwards (2018), Causes and consequences of 21st century ice sheet
401 melt. *Submitted*.
- 402 27. Le Bars, D., Drijfhout, S. & de Vries, H. A high-end sea-level rise probabilistic
403 projection including rapid Antarctic ice sheet mass loss. *Environ Res Lett* 12,
404 044013 (2017).
- 405 28. Golledge, N. R. *et al.* The multi-millennial Antarctic commitment to future sea-
406 level rise. *Nature* 526, 421–425 (2015).
- 407 29. Cornford, S. L. *et al.* Century-scale simulations of the response of the West
408 Antarctic Ice Sheet to a warming climate. *The Cryosphere* 9, 1579–1600–
409 (2015).
- 410 30. Wise, M. G., Dowdeswell, J. A., Jakobsson, M. & Larter, R. D. Evidence of
411 marine ice-cliff instability in Pine Island Bay from iceberg-keel plough marks.
412 *Nature* 550, 506–510 (2017).
- 413 31. Bell, R. E. *et al.* Antarctic ice shelf potentially stabilized by export of meltwater
414 in surface river. *Nature* 544, 344–348 (2017).
- 415 32. Kingslake, J., Ely, J. C., Das, I. & Bell, R. E. Widespread movement of
416 meltwater onto and across Antarctic ice shelves. *Nature* 544, 349–352 (2017).
- 417 33. Gourmelen, N. *et al.* Channelized Melting Drives Thinning Under a Rapidly
418 Melting Antarctic Ice Shelf. *Geophysical Research Letters* 17, 173 (2017).
- 419 34. Pattyn, F., Favier, L., Sun, S. & Durand, G. Progress in Numerical Modeling of
420 Antarctic Ice-Sheet Dynamics. *Curr Clim Change Rep* 3, 174–184 (2017).
- 421 35. Golledge *et al.* (2017), Antarctic climate and ice-sheet configuration during the
422 early Pliocene interglacial at 4.23 Ma, *Climate of the Past*, 13(7), pp.959–975.
- 423 36. Pukelsheim, F. The three sigma rule. *The American Statistician* 48, 88–91
424 (1994).
- 425 37. Miller, K. G. *et al.* High tide of the warm Pliocene: Implications of global sea-
426 level for Antarctic deglaciation. *Geology* 40, 407–410 (2012).
- 427 38. Raymo, M.E. *et al.*, 2018. The accuracy of mid-Pliocene $\delta^{18}\text{O}$ -based ice volume
428 and sea level reconstructions. *Earth-Science Reviews*, 177, pp.291–302.
- 429 39. Kopp, R. E., Simons, F. J., Mitrovica, J. X., Maloof, A. C. & Oppenheimer, M.
430 A probabilistic assessment of sea-level variations within the last interglacial
431 stage. *Geophysical Journal International* 193, 711–716 (2013).
- 432 40. Düsterhus, André, Tamisiea, M. E. & Jevrejeva, S. Estimating the sea-level
433 highstand during the Last Interglacial: a probabilistic massive ensemble

- 434 approach. *Geophysical Journal International* 206, 900–920 (2016).
435 41. Austermann, J., Mitrovica, J. X., Huybers, P. & Rovere, A. Detection of a
436 dynamic topography signal in last interglacial sea-level records. *Science*
437 *Advances* 3, 1–9 (2017).
438 42. Nias, I., Cornford, S. L. & Payne, A. J. Contrasting model sensitivity of the
439 Amundsen Sea embayment ice streams. *Journal of Glaciology* 62, 552–562
440 (2016).
441 43. Holden, P. B., Edwards, N. R., Oliver, K. I. C., Lenton, T. M. & Wilkinson, R.
442 D. A probabilistic calibration of climate sensitivity and terrestrial carbon change
443 in GENIE-1. *Climate Dynamics* 35, 785–806 (2009).
444 44. Edwards, N. R., Cameron, D. & Rougier, J. Precalibrating an intermediate
445 complexity climate model. *Climate Dynamics* 37, 1469–1482 (2011).
446 45. Nowicki, S. M. J. *et al.* Ice Sheet Model Intercomparison Project (ISMIP6)
447 contribution to CMIP6. *Geosci. Model Dev. Discuss.* 1–42 (2016).
448 doi:10.5194/gmd-2016-105-SC2
449

450 **Acknowledgements**

451 T.L.E., N.E. and P.H. were supported by EPSRC REsearch on Changes of Variability and
452 Environmental Risk (ReCoVER: EP/M008495/1) under the Quantifying Uncertainty in
453 ANTarctic Ice Sheet instability (QUAntIS) project (RFFLP 006). T.L.E. was also supported
454 by the EPSRC-funded Past Earth Network (EP/M008363/1) and the Université Joseph
455 Fourier – Grenoble International visitor fund ‘Campagne INVITES’. N.R.G is supported by
456 contract VUW1501 from the Royal Society Te Aparangi. I.N. was supported by the NERC
457 iSTAR-C project Dynamical control on the response of Pine Island Glacier (NE/J005738/1)
458 and now by the NASA Sea Level Change program. A.W. is supported by the Open
459 University Faculty of Science, Technology, Engineering and Mathematics.

460 Thanks to Rob DeConto for running additional simulations necessary for the analysis,
461 suggestions and helpful discussions, and to Kelsey Ruckert and Anders Levermann for
462 providing data. Thanks to the statisticians who attended the Past Earth Network events
463 ‘Assessing Palaeoclimate Uncertainty’ (held jointly with the Environmental Statistics Section
464 of the Royal Statistics Society, Cambridge, August 2016), ‘Emulators workshop’ (Leeds,
465 June 2017), and writing retreat (Callow Hall, August 2017) for their advice, particularly Ian
466 Vernon, Peter Challenor, and Jonty Rougier. Thanks to Dewi Le Bars, Doug McNeill, David
467 Demeritt and the King’s Geography Hazards, Risk and Regulation reading group (George
468 Adamson, Felicia Liu, Amar Razli, Laurence Ball and Ana Heilbron) for helpful comments
469 on the manuscript. Thanks to three anonymous reviewers for their comments and advice.
470 Thanks also to Dr Kai-Keen Shiu of the Gastrointestinal Oncology Unit at UCL Hospitals,
471 and to Dallas Campbell without whom this work would not have been possible.

472

473 **Author contributions**

474 T.L.E. conceived the idea, carried out the analysis, produced the figures, and wrote the
 475 manuscript. A.W. and P.B.H. performed preliminary analyses. A.J.P, A.W., C.R., G.D., I.N.,
 476 M.B. and N.R.G. contributed ideas on glaciological and oceanic aspects, while A.W., N.R.E.
 477 and P.B.H. contributed ideas on statistical aspects. All authors contributed to writing the
 478 manuscript.

479

480 **Author information**

481 The authors declare no competing financial interests. Correspondence and requests for
 482 materials should be addressed to T.L.E. (tamsin.edwards@kcl.ac.uk).

483

484 **Table 1. Probabilities from DeConto and Pollard (2016) study.** Means and standard deviations, and implied
 485 probability intervals, for DeConto and Pollard (2016) ensemble at 2100 for RCP8.5 for their four
 486 methodological choices (see text), using minimal assumptions about the distribution shape (finite mean and
 487 variance: Chebyshev inequality).

RCP8.5	LOW PLIOCENE		HIGH PLIOCENE	
	Bias	Bias	Bias	Bias
	Uncorrected	Corrected	Uncorrected	Corrected
Antarctic contribution at 2100 (cm sea-level equivalent)				
Mean \pm 1 s.d.	64 \pm 49	79 \pm 46	105 \pm 30	114 \pm 36
\geq 68% probability interval	[-22, 150]	[-2, 160]	[51, 158]	[51, 177]
\geq 90% probability interval	[-90, 217]	[-65, 223]	[9, 200]	[1, 227]

488

489

490 **Table 2. Projections for the Antarctic contribution to sea-level in 2100.** Calibrated with Pliocene, Last
 491 Interglacial and satellite data (1997-2017), with and without DeConto and Pollard (2016) marine ice cliff
 492 instability (MICI) parameterisation.

493

	RCP2.6		RCP4.5		RCP8.5	
	No MICI	MICI	No MICI	MICI	No MICI	MICI
Antarctic contribution at 2100 (cm sea-level equivalent)						
Mode	-6	15	0	24	15	45
Median	-1	19	5	46	21	79
Mean	0	20	7	49	22	83
68% interval	[-7, 8]	[4, 36]	[-1, 15]	[16, 83]	[13, 32]	[35, 133]
90% interval	[-9, 13]	[-3, 48]	[-3, 21]	[5, 103]	[9, 39]	[20, 157]
Exceedance probabilities						
≥ 30 cm	--	26%	--	68%	20%	88%
≥ 50 cm	--	4%	--	46%	--	71%
≥ 1 m	--	--	--	6%	--	36%

494

495

496 **Figure 1. Probabilistic projections of the Antarctic contribution to sea-level at 2100.** Projections estimated
497 under three RCPs, (a) with ice cliff instability parameterisation and (b) without, from emulation of the DeConto
498 and Pollard (2016) ice sheet model ensemble. Dotted lines are the uncalibrated emulator ensemble; solid lines
499 are calibrated with Last Interglacial and Pliocene reconstructions and satellite data from 1992-2017. Box and
500 whiskers show the [5, 25, 50, 75, 95]th percentiles; star shows the mode. The DeConto and Pollard (2016)
501 ensemble members for RCP8.5 (LowPliocene calibration; BiasCorrected and BiasUncorrected combined) are
502 shown as a histogram and mean \pm 2 s.d. interval in (a), scaled to the same height as the calibrated projection.
503 The projection for the Antarctic contribution due to ice discharge under the medium-high climate scenario A1B
504 by Ritz et al. (2015) is also shown in (b). Data from refs. 6 and 25 and supplementary simulations by R.
505 DeConto (pers. comm.) (see Methods).

506

507 **Figure 2. Emergence of ice cliff instability.** Projected 5-95% probability intervals for Antarctic sea-level
508 contributions this century, with and without the marine ice cliff instability (MICI) parameterisation of DeConto
509 and Pollard (2016). Data from refs. 6 and 25 and supplementary simulations by R. DeConto (pers. comm.) (see
510 Methods).

511

512 **Figure 3. Long-term projections of Antarctic sea-level contribution.** (a) Shaded/hatched regions: projected
513 5-95% intervals for Antarctic sea-level contribution to 2300 and for 2500 with (shaded) and without (hatched)
514 ice cliff instability (MICI) parameterisation under three greenhouse gas concentration scenarios. Dots: mode of
515 the RCP4.5 and RCP8.5 distributions with MICI. Single lines: range of results from Golledge et al. (2015) under
516 RCP8.5 (solid dark red), RCP8.5 with doubled atmosphere and ocean temperature changes (dashed purple),
517 RCP4.5 and RCP2.6 (solid black). Box and whisker at 2200 shows Ritz et al. (2015): [5, 25, 50, 75, 95]th
518 percentiles and mode (*). (b). Projected probability of exceeding 1 m Antarctic sea-level contribution over the
519 same period. Data from refs. 6 and 25 and supplementary simulations by R. DeConto (pers. comm.) (see
520 Methods).

521

522 **Figure 4. Multi-model comparison.** Projections from this study (bold text: 'EMULATED') at 2100 based on
523 emulation of DeConto and Pollard (2016) (with and without ice cliff instability, 'MICI'), along with results
524 from other probabilistic modelling studies. Box and whiskers show the [5, 25, 50, 75, 95]th percentiles; star
525 shows the mode. Numbers show the median, [5th, 95th] percentiles and, where available, the mode (*). "High
526 Scenarios" (pink/red) are for high-end (RCP8.5) or medium-high (Special Report on Emissions Scenario A1B¹)
527 greenhouse gas emissions or concentrations, or immediate collapse of part of West Antarctica (Little et al.
528 (2013): 5th percentile and median are estimated from digitisation); Levermann et al. (2014) is from models with
529 ice shelves, without time delay. "Low Scenarios" (grey/black) are for low greenhouse gas concentrations
530 (RCP2.6) or other baseline case (Little et al., 2013); Levermann et al. (2014) is with time delay. Levermann et
531 al. (2014) and Ritz et al. (2015) are for ice discharge contribution only. Data from refs. 2-6 and 25,
532 supplementary simulations by R. DeConto (pers. comm.), and mode for ref. 5 supplied by K.L. Ruckert (pers.
533 comm) (see Methods).

534

535

536 **METHODS**

537 **Simulator ensemble design**

538 DeConto and Pollard (2016) perturb three continuous parameters, sampling four levels for
539 each in a factorial design to generate $4^3 = 64$ ensemble members:

540 **OCFAC:** Ocean melt factor, which controls sub-ice-shelf direct melting. Defined as a
541 factor by which the default value is multiplied. $OCFAC = \{0.1, 1, 3 \text{ and } 10\} \times 0.224 \text{ m yr}^{-1}$
542 $^{\circ}\text{C}^{-2}$. (Note that DP16 quotes incorrect units of $\text{m yr}^{-2} \text{ }^{\circ}\text{C}^{-2}$ in two places).

543 **CREVLIQ:** Crevasse liquid depth, which controls ice shelf collapse by hydrofracturing
544 due to surface liquid. Defined as the additional crevasse depth due to surface melt plus
545 rainfall rate. $CREVLIQ = \{0, 50, 100, 150\} \text{ m per } (\text{m yr}^{-1})^{-2}$.

546 **VCLIF:** Maximum net ice wastage rate. Controls cliff failure after ice shelf collapse.
547 $VCLIF = \{0, 1, 3, 5\} \text{ km yr}^{-1}$.

548 For present day and future projections, this ensemble is duplicated with the ocean bias
549 correction applied. When emulating the ice sheet model (see below) we combine these 128
550 ensemble members and treat the bias correction as a continuous uncertain parameter:

551 **BIAS:** Southern Ocean bias correction applied to present day and future simulations.
552 Defined as a scalar ranging from 0 (no bias correction, $+0^{\circ}\text{C}$) to 1 (full bias correction,
553 $+3^{\circ}\text{C}$). Active only for present day and future simulations.

554 We use time series data for the ensemble provided by Rob DeConto. When emulating
555 the model, we found a sign error in the DP16 Supplementary Information: the Last
556 Interglacial value for simulation row 6 ($OCFAC = 0.1$, $CREVLIQ = 50$, $VCLIF = 1$) should
557 be $+2.63 \text{ m}$, not -2.63 m .

558

559 **Building the emulators**

560 We use Gaussian Process regression ('kriging' when used for spatial interpolation), because
561 it is flexible, non-parametric, and provides uncertainty estimates⁴⁶. As usual for emulation of
562 computer models, we set the 'nugget' to zero because the ice sheet model is deterministic.
563 We refer to 'the emulator' in the main text for simplicity, but this comprises separate
564 emulators for each scalar output: Pliocene and LIG sea-level change, present day (1992-2017
565 change in the RCP4.5 simulation) and the change from 2000 to every even-numbered year up
566 to 2500 for the three RCPs. We construct, validate, calibrate and make predictions using the
567 R software packages DiceKriging and a modified version of DiceEvaluation.

568 Let the function $f(x)$ be the ice sheet model, which simulates sea-level change in a
569 particular era (e.g. the Pliocene) as a function of the set of its input parameters, x . We

570 consider only one output at a time, to avoid the need for a further index. An emulator $f_{em}(x)$
571 for a particular output of $f(x)$ can be written as:

$$f_{em}(x) = \sum_j \beta_j g_j(x) + u(x)$$

572 where $g_j(x)$ are known functions of x , β_j are regression coefficients, and $u(x)$ is a stochastic
573 process with a specified covariance function. We wish to select the subset of x that has the
574 most influence on $f_{em}(x)$.
575

576 Design and validation of the emulators comprises two parts: a step-wise model
577 selection procedure, to choose the mean function (i.e. which simulator parameters, and
578 interactions between these, to use as regressors), and a ‘leave-one-out’ (LOO) cross-
579 validation procedure, to evaluate which is the most suitable covariance function and whether
580 each emulator is sufficiently accurate for our purposes. We perform these procedures for six
581 outputs — the two palaeo-eras, the present day, and the three RCP projections at 2100 — to
582 choose the overall emulator structure. The final fitting of the emulators with the full ensemble
583 data, and their use for prediction, are discussed later.

584

585 *Mean functions:* There are important interactions between parameters — for example,
586 increasing the bias correction (BIAS) increases the effect of maximum ice wastage rate
587 (VCLIF) on projections — but we also wish to avoid over-fitting by including too many
588 interaction terms. We use the R MASS package’s stepAIC to select model terms, testing up
589 to second order (three-way) interactions between parameters, using Bayesian Information
590 Criterion because it is generally more parsimonious than Akaike Information Criterion. The
591 resulting mean functions for the six outputs are:

592

593 Pliocene and Last Interglacial:

594 $g_{\text{palaeo}}(\mathbf{x}) \sim (\text{OCFAC}, \text{CREVLIQ}, \text{VCLIF}, \text{CREVLIQ}*\text{VCLIF})$

595

596 Present day and RCP2.6 at 2100:

597 $g_{\text{low}}(\mathbf{x}) \sim (\text{OCFAC}, \text{CREVLIQ}, \text{VCLIF}, \text{BIAS}, \text{OCFAC}*\text{VCLIF}, \text{OCFAC}*\text{BIAS},$
598 $\text{CREVLIQ}*\text{VCLIF}, \text{VCLIF}*\text{BIAS}, \text{OCFAC}*\text{VCLIF}*\text{BIAS})$

599

600 RCP4.5 and RCP8.5 at 2100:

601 $g_{\text{high}}(\mathbf{x}) \sim (\text{OCFAC}, \text{CREVLIQ}, \text{VCLIF}, \text{BIAS}, \text{OCFAC}*\text{VCLIF}, \text{OCFAC}*\text{BIAS},$
602 $\text{CREVLIQ}*\text{VCLIF})$

603

604 where $g \sim (a,b)$ means g is a linear function of a and b , etc, and $a*b$ indicates an interaction
 605 term.

606

607 *Covariance functions:* The covariance controls the smoothness between data points, with a
 608 trade-off between accuracy and over-fitting. We compare the success of different covariance
 609 functions — Matern(5/2), Matern(3/2), exponential, and power-exponential (exponential
 610 family, where the exponent can vary between 0 and 2) — using the mean function selected
 611 above, and choose the one with the smallest normalised Euclidean distance in a LOO
 612 procedure. The LOO procedure comprises fitting the emulator to all ensemble members
 613 except one (i.e. 63 of 64 for Pliocene and LIG; 127 of 128 for present and future), and then
 614 predicting the final member to compare with the simulation itself. This is repeated for all
 615 combinations ($N_{\text{ens}} = 64$ or 128) to provide a summary statistic. Normalised Euclidean
 616 distance is:

$$d = \sqrt{\sum_{i=1}^{N_{\text{ens}}} \frac{(f_{\text{em}}(x_i) - f(x_i))^2}{\sigma_{\text{em}:x_i}^2}}$$

617

618 where i is the ensemble member and σ_{em} is the emulator error for that prediction. We choose
 619 this metric because it makes use of the uncertainty estimate inherent in a Gaussian Process
 620 emulator to standardise the residuals, so that an emulator with some large errors is not overly
 621 penalised if it has sufficiently large uncertainty estimates to generally encompass the true
 622 value. This also guards against overfitting, by penalising too-confident emulators. The
 623 distance metric therefore balances the two aims of emulator accuracy and appropriate
 624 confidence. The resulting covariance functions from this procedure are power-exponential for
 625 the LIG, Matern(3/2) for 1992-2017, and exponential for the Pliocene and future outputs.

626

627 **Validating and fitting the emulators**

628 We use various validation outputs to assess emulator adequacy: RMSE; Kendall's tau, a non-
 629 parametric measure of correlation, for the emulator predictions versus the simulations; and
 630 the fraction of predictions for which the simulation lies within the emulator 95% credibility
 631 interval, for which values lower than ~90% would indicate an over-confident emulator (i.e.
 632 too-small uncertainty estimates). The RMSE and Kendall rank correlation coefficients
 633 between the emulator predictions and simulations are 12 cm (1.4% of the data range) and
 634 0.958 respectively for the Pliocene; 26 cm (2.7%) and 0.923 for the Last Interglacial; 0.1 cm
 635 (0.6%) and 0.972 for the present day, and 0.9-1.2 cm (0.4-0.8%) and 0.973-0.976 for the

636 three future projection emulators, indicating sufficient accuracy. The fraction of predictions
637 within the emulator 95% interval is 100% for the Pliocene, 89% for the LIG, and 91-98% for
638 the present and future, indicating sufficiently large emulator uncertainty estimates. The
639 predictive accuracy and uncertainty estimates of the six emulators can also be inspected
640 visually by plotting the emulator predictions vs simulations and the standardised residuals
641 (Extended Data Figure 6).

642 Having judged these six emulators to be adequate, we fit each emulator with the full
643 ensemble for that output. We use the emulator structures for the year 2100 for all timeslices
644 for that RCP.

645

646 **Emulator ensemble design**

647 We predict 10,000 points in the parameter space using a maximin Latin Hypercube (i.e.
648 efficiently space-filling) design. The MICI design samples from uniform distributions for all
649 four parameters, based on discussion with one of the original DP16 authors (DeConto, pers.
650 comm.); the No-MICI design has VCLIF set to zero. The effect of VCLIF, CREVLIQ and
651 OCFAC on sea-level contribution at 2100 under RCP8.5 in the MICI case is shown in
652 Extended Data Figure 7, which shows the strong dependence on VCLIF. The reason for some
653 apparent gaps in emulator coverage is that the ensemble design is space-filling but does not
654 necessarily sample points in each corner of the parameter space, as the original ensemble
655 members do.

656

657 **Pliocene calibration**

658 The LowPliocene and HighPliocene projections of DP16 are presented (and have been
659 interpreted by others^{27,47}) as equally plausible, but here we make the case that the
660 HighPliocene calibration is not robust. This is important because the RCP8.5 projections are
661 uniquely sensitive to the particular minimum value chosen for the HighPliocene constraint
662 (10 m). Extended Data Figure 2a and b show that when the lower bound exceeds 9.6 m, this
663 results in much higher means and much smaller standard deviations, because fewer than a
664 quarter of the ensemble members pass. The sensitivity is caused by a combination of the
665 small ensemble size and the strong correlation in the model between Pliocene sea-level and
666 RCP8.5 projections (large circles in Extended Data Figure 3a).

667 This sensitivity to the Pliocene lower bound is exacerbated by the choice of calibration
668 method: a simple ‘accept’ or ‘reject’, which can be expressed in the ‘history matching’
669 framework^{22,48} below. This binary filtering means we should choose a sufficiently wide range
670 of tolerance, because every rejected ensemble member is treated as completely implausible

671 (by being removed, rather than down-weighted as in Bayesian calibration). Treating two
672 ranges as equally plausible is not coherent, because it implies values in the range 5–10 m and
673 15-20 m are simultaneously both plausible and implausible. The chosen data range should be
674 both broad and unique to obtain a calibration that is robust and meaningful.

675 Gasson, DeConto and Pollard (2016)²⁰ estimate the Antarctic contribution to mid-
676 Pliocene sea-level has a maximum of 13 m, which would rule out most of the HighPliocene
677 range, suggesting the interval 10-20 m is not well supported. (A range of 10-13 m would be
678 inconsistent with the large degree of uncertainty in Pliocene reconstructions^{37,49})

679 In fact, increasing the upper bound from 13 m would have no effect, because the
680 maximum Pliocene change in the ensemble is 12.4 m. Decreasing the lower bound below 5 m
681 would also make little difference, because the original (no discrepancy) DP16 Last
682 Interglacial calibration (3.5-7.4 m) rejects these ensemble members: none of the ensemble
683 members that pass the LIG constraint have Pliocene sea-level changes of less than 5 m
684 (Extended Data Figure 4: no large circles directly below shaded box). The crucial judgement
685 is therefore whether the 10 m HighPliocene lower bound can be justified.

686 We conclude that Pliocene Antarctic sea-level contribution is currently too uncertain to
687 use the HighPliocene constraint, particularly for this model and for a history matching
688 approach, and that the LowPliocene calibration is far more robust.

689

690 **Model discrepancy**

691 Model ‘discrepancy’, or ‘structural error’, is defined as the smallest possible difference
692 between a model simulation and the true values: that is, how well the model could reproduce
693 reality at its best possible, ‘tuned’, parameter values^{4,21,22,23}. Discrepancy is an essential part
694 of model calibration: not incorporating it implies that a model could be tuned to perfectly
695 match reality. Using a value less than the observational error would imply we could simulate
696 reality better than we could measure it. Model discrepancy can, in some cases, be
697 approximately estimated by comparing simulations with multiple observations. But if there
698 are insufficient observations to do this, as is the case here, discrepancy can be viewed as a
699 tolerance to model error⁴⁸ estimated by expert judgement^{4,24} (see below).

700

701 **Calibrating projections**

702 We re-express the DP16 calibration within a history matching framework, extending it to
703 account for emulator error and model discrepancy. We adapt notation by Vernon et al.
704 (2010)⁵⁰ here. The relationship between a palaeodata reconstruction or an observation of sea-
705 level change (Pliocene, LIG, or 1992-2017 trend), z , and the true value, y , is modelled as:

706

$$z = y + \epsilon_{obs}$$

707

where ϵ_{obs} has variance σ_{obs}^2 , the square of the observational or palaeodata reconstruction

708

error. The relationship between the true value and the simulation of this sea-level change is:

709

$$y = f(x^*) + \epsilon_{md}$$

710

where x^* are the best values of the parameters, and ϵ_{md} is the model discrepancy with

711

variance σ_{md}^2 . We emulate $f(x)$:

712

$$f(x) = f_{em}(x) + \epsilon_{em:x}$$

713

714

where $f_{em}(x)$ is the mean emulator prediction for $f(x)$, and $\epsilon_{em:x}$ is the emulator error as

715

before; it varies with x , and is automatically estimated in Gaussian Process emulation. For a

716

given emulated output (Pliocene, LIG, 1992-2017 trend) we can use the standardised

717

distance, also known as *implausibility*, I :

718

$$\mathcal{I}^2(x) = \frac{(f_{em}(x) - z)^2}{\sigma_{obs}^2 + \sigma_{em:x}^2 + \sigma_{md}^2}$$

719

to accept or reject a given emulated ensemble member with parameter values x . We interpret

720

the accepted ensemble members as a posterior probability distribution. This represents a

721

judgement that this distribution represents our uncertainty about future sea-level rise (given

722

the limitations of the ice sheet model and palaeodata), i.e. that the parameter space outside the

723

calibration intervals has a low probability of being plausible.

724

We use a minimum LIG palaeodata value of 3.5 m, rather than the 3.6 m quoted by

725

DP16, for consistency with their calibrated ensemble results which include a member with

726

LIG sea-level change of 3.53 m.

727

The palaeodata reconstruction errors are not defined. We conservatively treat the

728

DP16 range as a mean \pm 1 s.d. interval, so use $\sigma_{obs} = \{5, 2\}$ m for the Pliocene and LIG

729

respectively. The observational constraint (Shepherd et al., 2018)²⁵ is the cumulative mass

730

loss from 1992-2017, (2720 ± 1390) Gt, converted to cm sea-level equivalent by dividing by

731

3600, to give (0.756 ± 0.386) cm sea-level contribution over this period. Model discrepancy

732

is set to $\sigma_{md} = 0.5$ cm for 1992-2017 sea-level change.

733 When calibrating with palaeodata, we accept ensemble members with $I < 1$ for the
734 Pliocene and LIG, so that the simplest case without emulator and model errors matches the
735 interval used by DP16. We note this Pliocene range approximately corresponds to a 95%
736 interval in some reconstructions, but the LIG range may correspond to a lower probability
737 than 95% by some estimates, and so may be too strict a constraint (see main text). Calibration
738 with satellite data observations accepts ensemble members with $I < 3$, to follow the usual
739 history matching convention for well-defined errors: for a smooth unimodal distribution, $I <$
740 3 with probability greater than or equal to 95% (Pukelsheim, 1994)³⁶; for Gaussian
741 distributions, as we expect for the satellite data errors, the probability interval is 99.7%.

742 Extended Data Figure 3 shows the ‘calibration relationships’ for RCP8.5 at 2100: the
743 relationships between past and future. Grey boxes show the original palaeodata constraints;
744 dashed lines show the broader intervals after accounting for model discrepancy. Accounting
745 for emulator error in the implausibility means that some emulator ensemble members are
746 accepted that lie just outside the calibration interval.

747 Percentiles and exceedance probabilities are estimated directly from the 10,000-
748 member emulator ensemble, and modes from kernel density estimation using an automatic
749 (Silverman) bandwidth. We do not include emulator uncertainties in the distributions; these
750 are small at 2100, but increase on multi-century timescales so would broaden these
751 distributions. To improve the clarity of Figure 3, we exclude 1, 3 and 5 data points from each
752 of RCP8.5, RCP4.5 and RCP2.6 MICI projections respectively, because the estimates are not
753 continuous in time (due to slight differences in emulator fitting).

754

755 **Multi-model comparisons**

756 We show distributions from Ruckert et al. (2016)⁵ provided by Kelsey Ruckert, and estimate
757 the distribution at 2100 for Little et al. (2013)² by digitisation of the original figures. We re-
758 estimate the modes for Ritz et al. (2015)⁴ distributions using an automatic bandwidth for the
759 kernel density estimation, rather than the broader, fixed bandwidth used in the original study.
760 We assume differences due to definitions of time period are small enough to be ignored: all
761 are 2000-2100, except Little et al. (2013)² (1990-2099) and the IPCC¹ (1986–2005 to 2081–
762 2100 for Antarctic component).

763

764 **Palaeodata uncertainties**

765 We here consider probability intervals for palaeodata constraints. Peak total sea-level change
766 for the LIG estimated by Kopp et al. (2013)³⁹ is 6.4-10.9 m (90% probability interval), and by
767 Dusterhus et al. (2016)⁴⁰ is 6.1-16.7m (80% probability). These broadly encompass recent

768 assessments that the upper end of the widely used 6-9 m range⁴⁹ could increase by several
769 metres⁴¹. Subtracting a range of estimates for the contributions from Greenland, thermal
770 expansion and glaciers in the same way as Ruckert et al. (2016)⁵ (3.4-4.8 m) gives Antarctic
771 contributions of 1.6-7.5 m and 1.3-13.3 m respectively.

772 For the Pliocene, Miller et al. (2012)³⁷ estimate 22 ± 10 m (95% range) total sea-level
773 change; subtracting 7 m for the Greenland ice sheet and 1 m for thermal expansion (Golledge
774 et al., 2017)³⁵ would imply approximately 14 ± 10 m Antarctic contribution, i.e. 4-24 m.
775 There is no difference between using a combined 5-25 m range and using the LowPliocene
776 (5-15 m) constraint presented here, because the DP16 ensemble maximum is 12.4 m, though
777 for a different model or ensemble design the upper bound might have more influence.
778 Golledge et al. (2017)³⁵ estimate 8.6 ± 2.8 m for the Antarctic contribution to the early
779 Pliocene, and we use their Gaussian assumption to derive the 95% (2σ) range.

780

781 **Code availability**

782 All emulation was performed in R using the DiceKriging and DiceEvaluation packages with
783 minor modifications by TLE. The scripts and input data for the main analysis (sea-level
784 projections at 2100) are available as a downloadable R package on GitHub
785 (<https://github.com/tamsinedwards/revisitmici>, v1.0.2) and can be run without installation on
786 the cloud-based computational reproducibility platform Code Ocean at
787 <https://doi.org/10.24433/CO.4ebd8cda-35c0-4d8f-9b7c-d1b064109437>.

788

789 **Data availability**

790 All projections from this study are available on request. Simulations of the LIG and Pliocene,
791 1992-2017 mean and 2100 sea level change for all DP16 ensemble members are available in
792 the Code Ocean data folder at the above link. Simulations at 2500 for the subset of the DP16
793 ensemble passing their calibration are available also in the Supplementary Materials of
794 DeConto and Pollard (2016).

795

796 **Methods References**

797

- 798 46. O'Hagan, A. Bayesian analysis of computer code outputs: A tutorial. *Reliability*
799 *Engineering and System Safety* 91, 1290–1300 (2006).
800 47. Sweet, W. V. *et al.* GLOBAL AND REGIONAL SEA-LEVEL RISE
801 SCENARIOS FOR THE UNITED STATES. 1–75 (2017).
802 48. Williamson, D. *et al.* History matching for exploring and reducing climate model
803 parameter space using observations and a large perturbed physics ensemble.
804 *Climate Dynamics* 41, 1703–1729 (2013).

- 805 49. Dutton, A. *et al.* Sea-level rise due to polar ice-sheet mass loss during past warm
806 periods. *Science* 349, aaa4019–aaa4019 (2015).
- 807 50. Vernon, I., Goldstein, M. & Bower, R. G. Galaxy Formation: a Bayesian
808 Uncertainty Analysis. *Bayesian Analysis* 5, 619–669 (2010).

809 **Extended Data**

810

811 **Extended Data Figure 1. Sensitivity of DeConto and Pollard RCP8.5 projections to Pliocene data lower**
812 **bound.** DeConto and Pollard (2016) BiasUncorrected (a) and BiasCorrected (b) projections for Antarctic sea-
813 level contribution by 2100 under RCP8.5 as a function of the lower bound of the Pliocene data range. Mean \pm 1
814 s.d. range shown as central solid line with pink shading; mean \pm 2 s.d. range as dotted line. (c) Sensitivity of
815 emulated projections for RCP8.5 at 2100 with MICI from this study: [5, 25, 50, 75, 95]th percentiles and mode
816 (*). Data from ref. 6.

817

818 **Extended Data Figure 2. DeConto and Pollard RCP8.5 projection distributions.** DeConto and Pollard
819 (2016) ensemble projections for Antarctic sea-level contribution by 2100 under RCP8.5 for their four variants,
820 LowPliocene BiasUncorrected (a) and BiasCorrected (b), and High Pliocene similarly (c, d), showing the full
821 64-member ensemble and the subset selected by calibrating with Pliocene and Last Interglacial sea-level
822 reconstructions. The mean \pm 1 s.d. range of the ensemble is shown as a solid red line with pink shading, and the
823 68% or greater probability interval is shown as a horizontal black line (see main text and Methods for more
824 details). Data from ref. 6.

825

826 **Extended Data Figure 3. Relationships between RCP8.5 projections at 2100 and past sea-level changes.**
827 Sea-level contribution at 2100 under RCP8.5 versus (a) Pliocene sea-level change; (b) Last Interglacial sea-level
828 change; (c) sea-level change from 1992-2017, for the emulator (small grey dots) and DP16 simulator (large open
829 circles) with ocean bias correction off (blue) and on (red). Grey shading indicates the DP16 palaeodata range (a,
830 b) or observational mean \pm 3 s.d. (c); the dashed line additionally includes model error. Data from refs. 6 and 25
831 and supplementary simulations by R. DeConto (pers. comm.) (see Methods).

832

833 **Extended Data Figure 4. Relationship between past and future sea-level changes with and without MICI.**
834 Simulator ensemble (large circles), and emulated ensembles (small circles) with (a) cliff instability and (b) no
835 cliff instability, showing Pliocene versus Last Interglacial sea-level changes and shaded by sea-level
836 contribution at 2100 under RCP8.5. Large emulator points and filled simulator points pass the 1992-2017
837 calibration. Shaded rectangle indicates bounds of DP16 LowPliocene and Last Interglacial palaeodata
838 constraints; dashed box shows constraints in this study, i.e. including model error. Data from refs. 6 and 25 and
839 supplementary simulations by R. DeConto (pers. comm.) (see Methods).

840

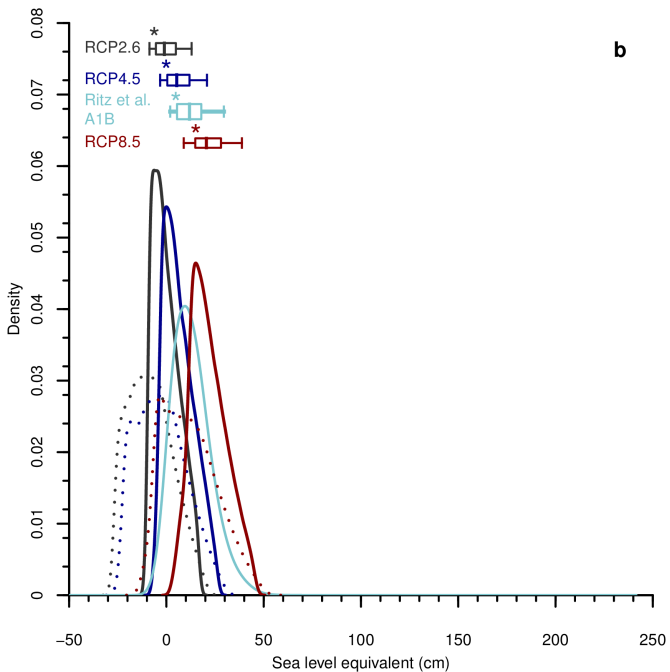
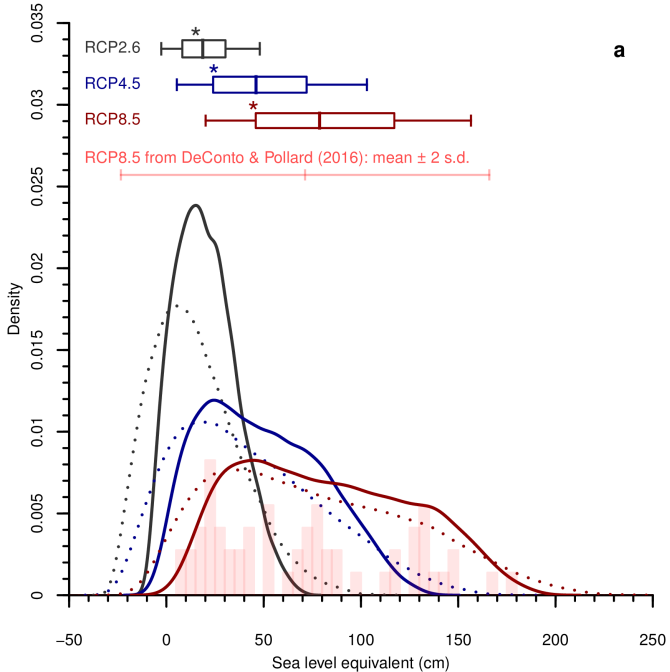
841 **Extended Data Figure 5. Sensitivity of RCP8.5 projections to MICI and calibration choices.** Projections for
842 RCP8.5 at 2100, with and without MICI, for different combinations of calibration eras ('palaeo': Pliocene and
843 Last Interglacial; present: 1992-2017) and model discrepancy (with, without, and double). Box and whiskers
844 show the [5, 25, 50, 75, 95]th percentiles; star shows the mode. Numbers show the median, [5th, 95th] percentiles
845 and mode (*). Data from refs. 6 and 25 and supplementary simulations by R. DeConto (pers. comm.) (see
846 Methods).

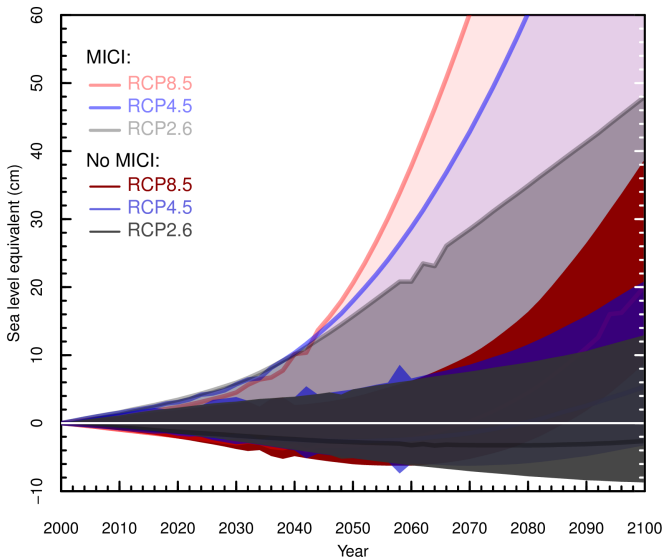
847

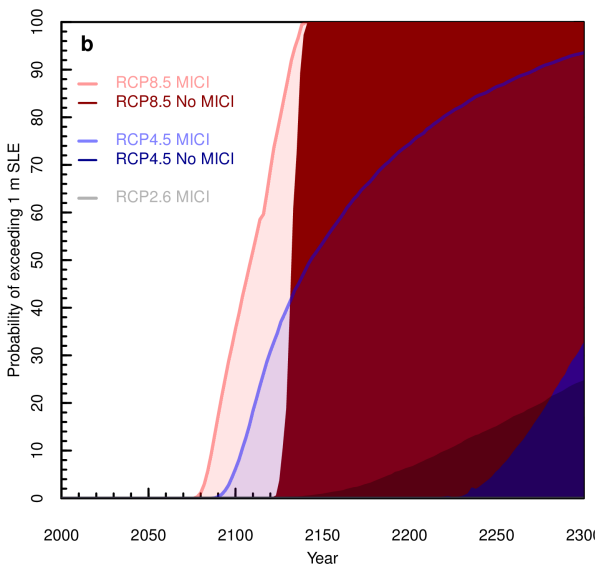
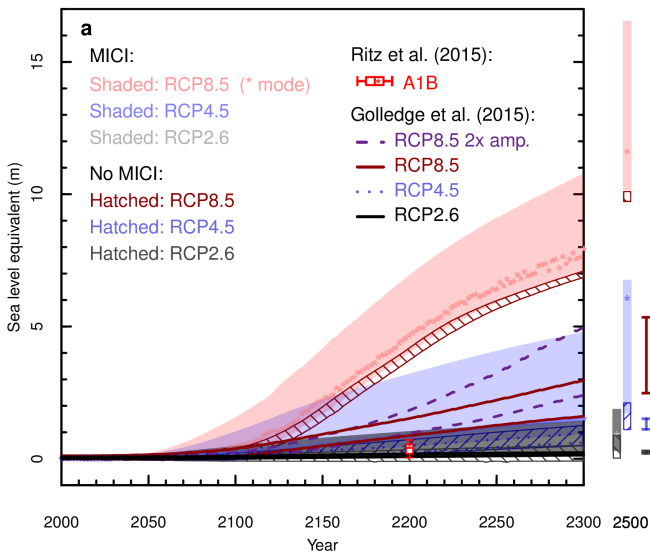
848 **Extended Data Figure 6. Emulator validation.** Left column: Emulator prediction versus simulation for each
849 ensemble member, with the emulator fitted to the other ensemble members, for each of the outputs used for

850 building and validating emulator structure: RCP8.5, RCP4.5, and RCP2.6 sea-level contribution at 2100; 1992-
851 2017 contribution; Last Interglacial; and Pliocene. Vertical error bars show 95% credibility intervals. Right
852 column: Difference between emulator predictions and simulations, standardised by emulator error, for the same
853 six outputs. Values falling mostly between ± 2 indicate the emulator has adequate uncertainty estimates. Data
854 from ref. 6 and supplementary simulations by R. DeConto (pers. comm.) (see Methods).

855
856 **Extended Data Figure 7. Sensitivity of RCP8.5 projections to model parameters.** Sea-level contribution at
857 2100 under RCP8.5 versus VCLIF (a), CREVLIQ (b) and OCFAC (c) parameters for emulator (small grey dots
858 with error bars) and simulator (large open circles: BiasUncorrected blue, BiasCorrected red). Data from ref. 6
859 and supplementary simulations by R. DeConto (pers. comm.) (see Methods).







HIGH SCENARIOS

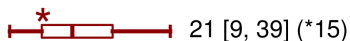
With MICI:

DeConto & Pollard (2016): EMULATED RCP8.5

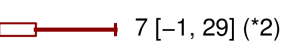


Without MICI:

DeConto & Pollard (2016): EMULATED RCP8.5



Ruckert et al. (2016)
RCP8.5



Little et al. (2013)
Immediate collapse



Ritz et al. (2015): dynamic only
A1B



Levermann et al. (2014): dynamic only
RCP8.5 without time delay



LOW SCENARIOS

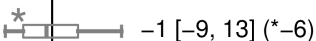
With MICI:

DeConto and Pollard (2016): EMULATED RCP2.6

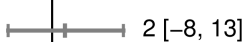


Without MICI:

DeConto and Pollard (2016): EMULATED RCP2.6



Little et al. (2013)
Base case



Levermann et al. (2014): dynamic only
RCP2.6 with time delay



-50

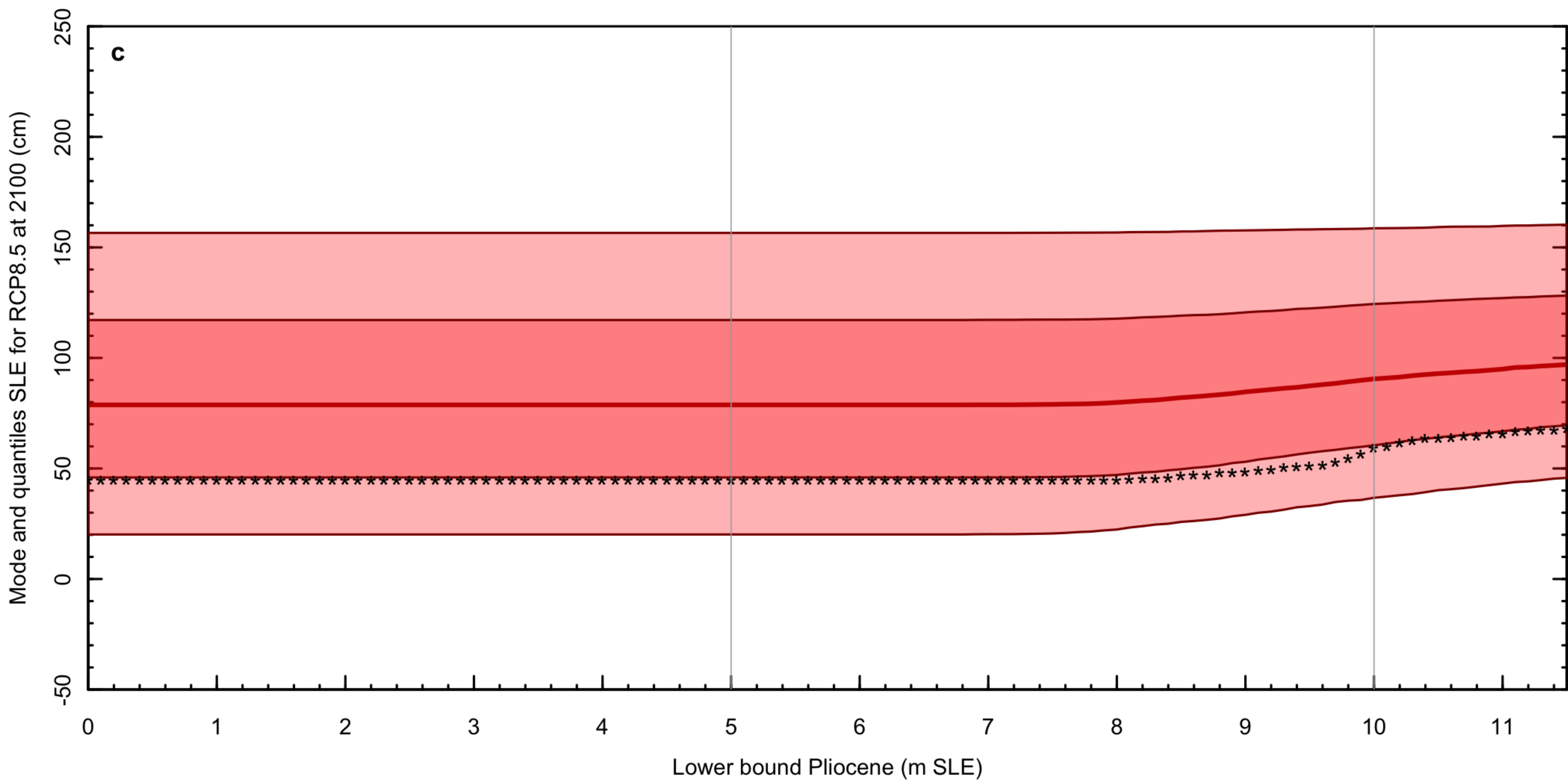
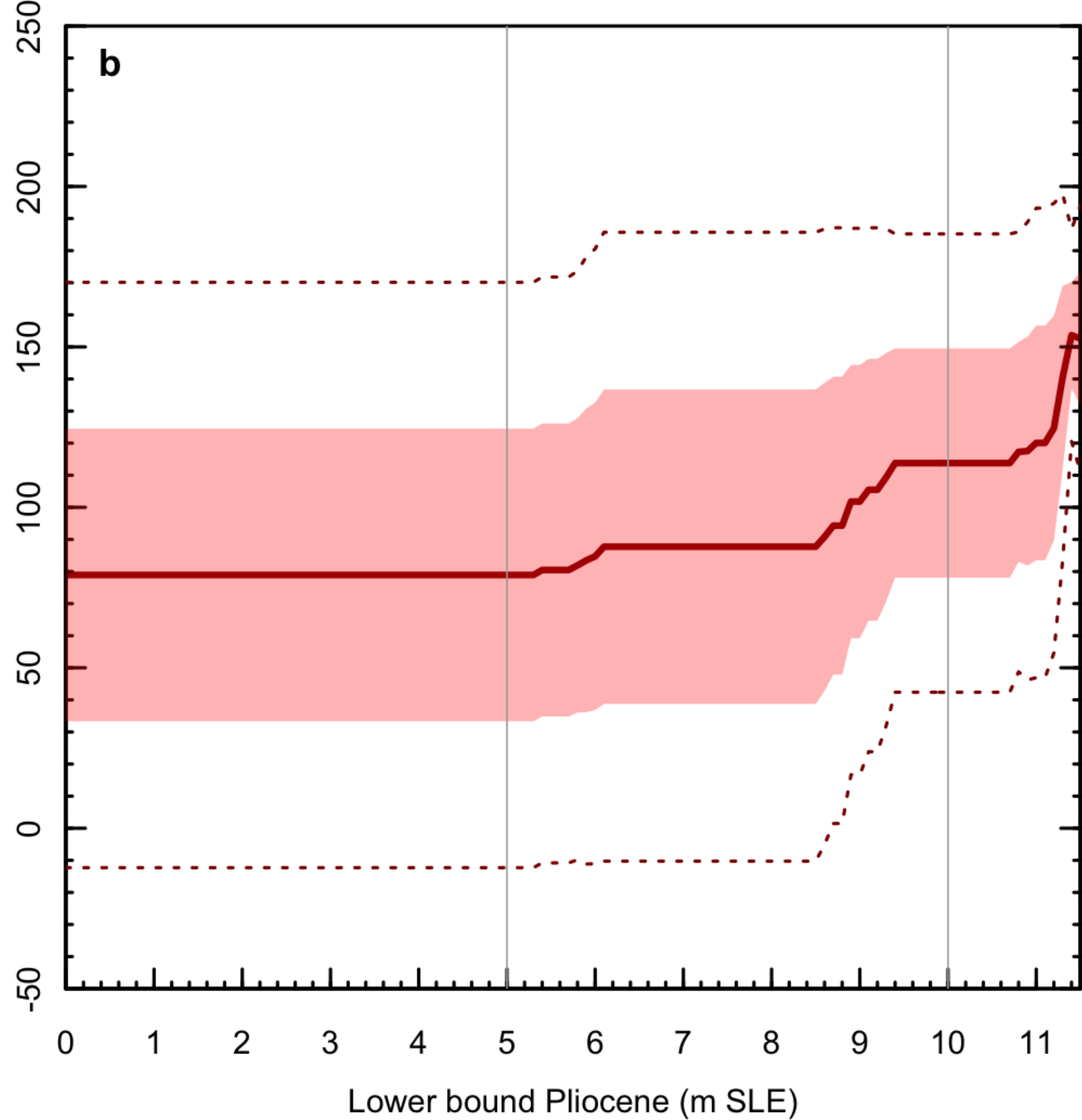
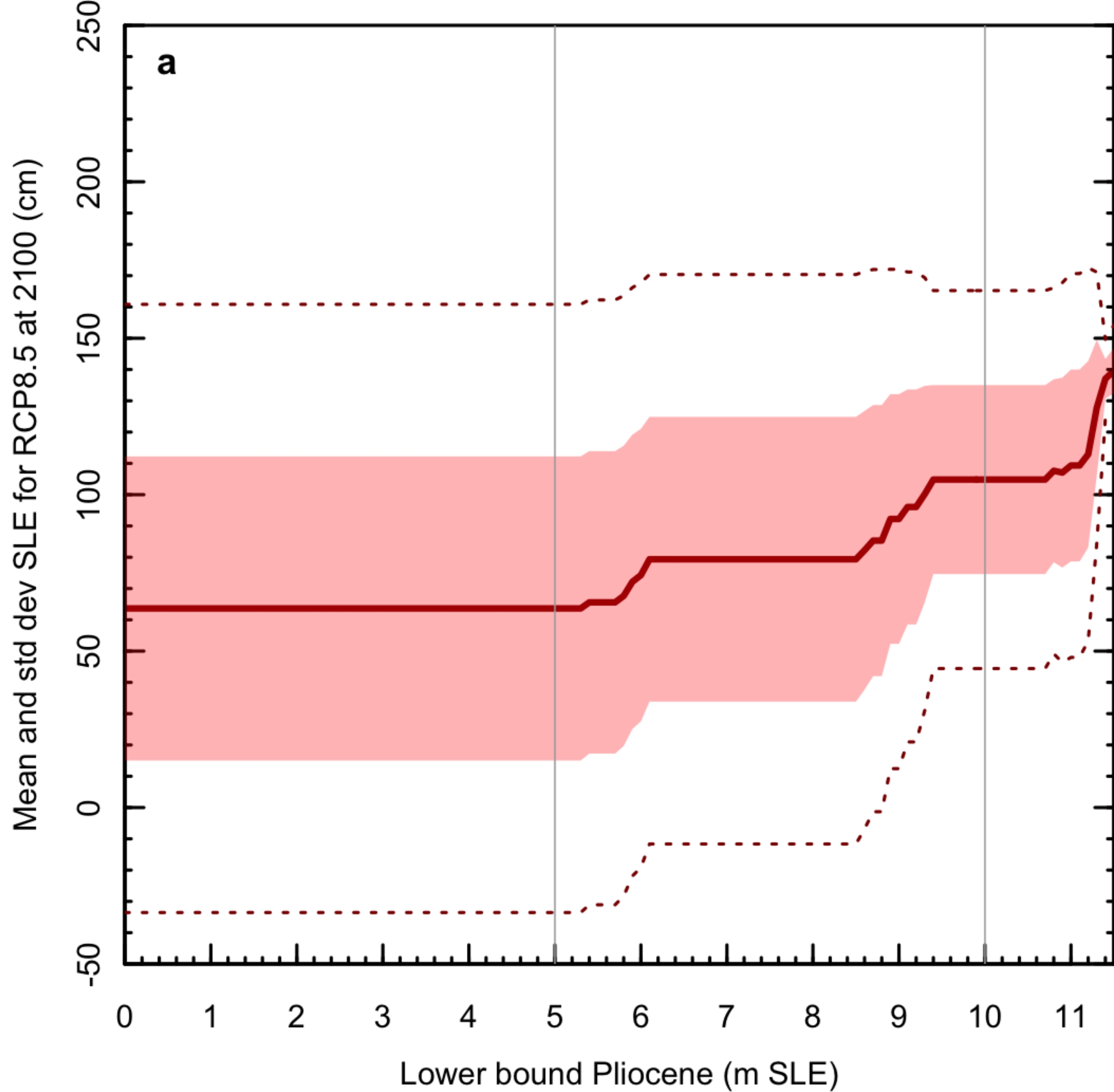
Sea level equivalent at 2100 (cm)

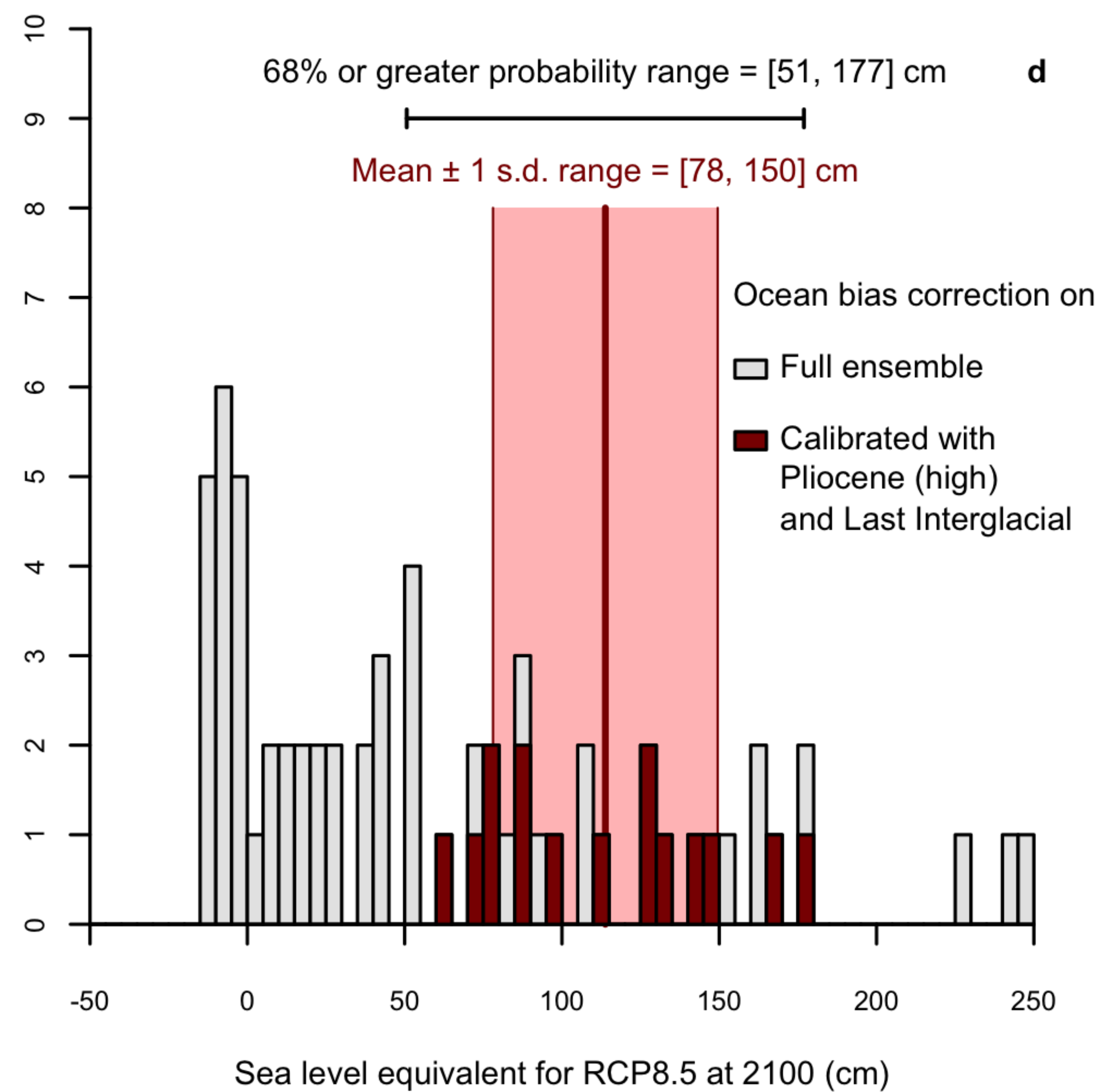
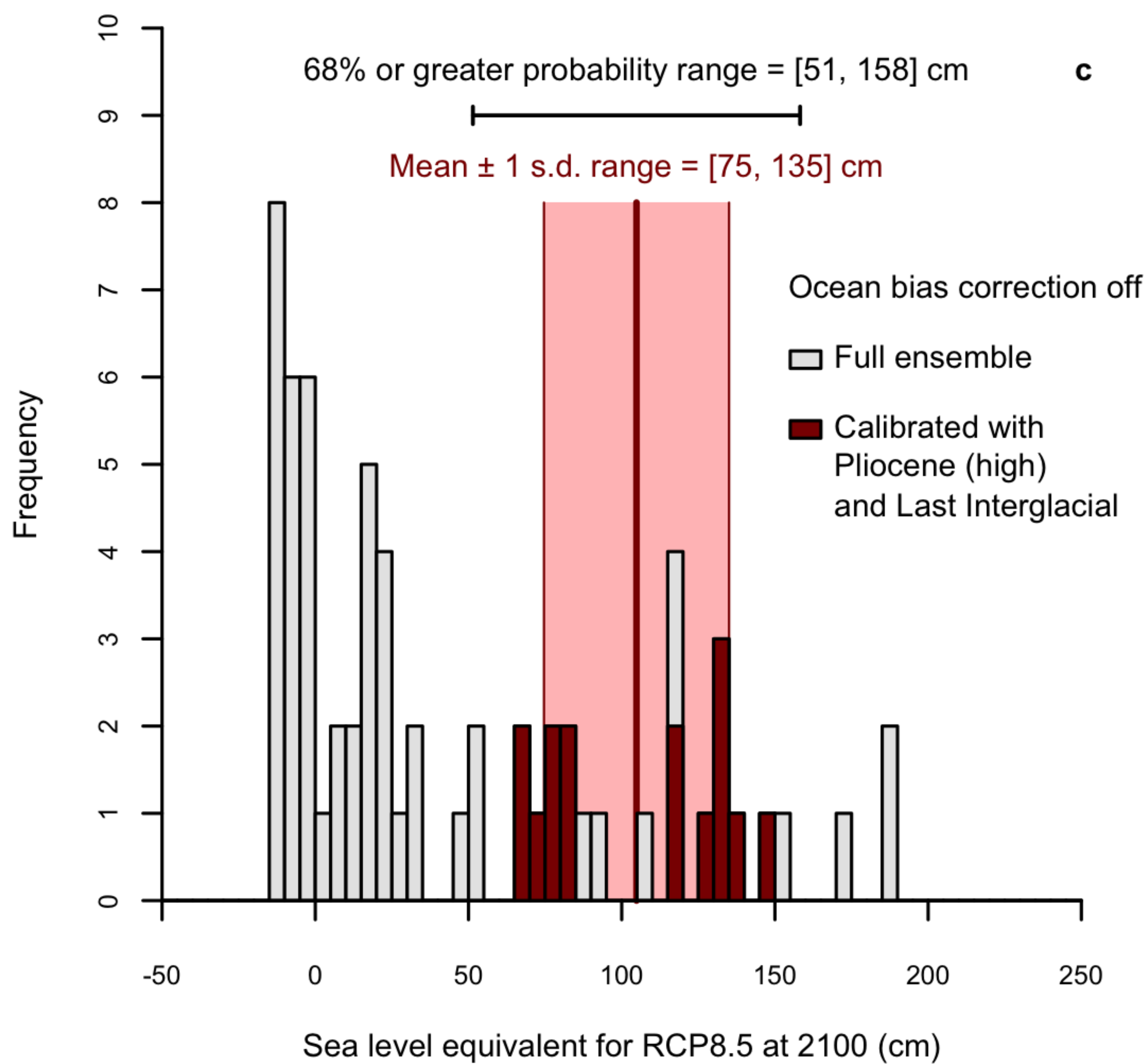
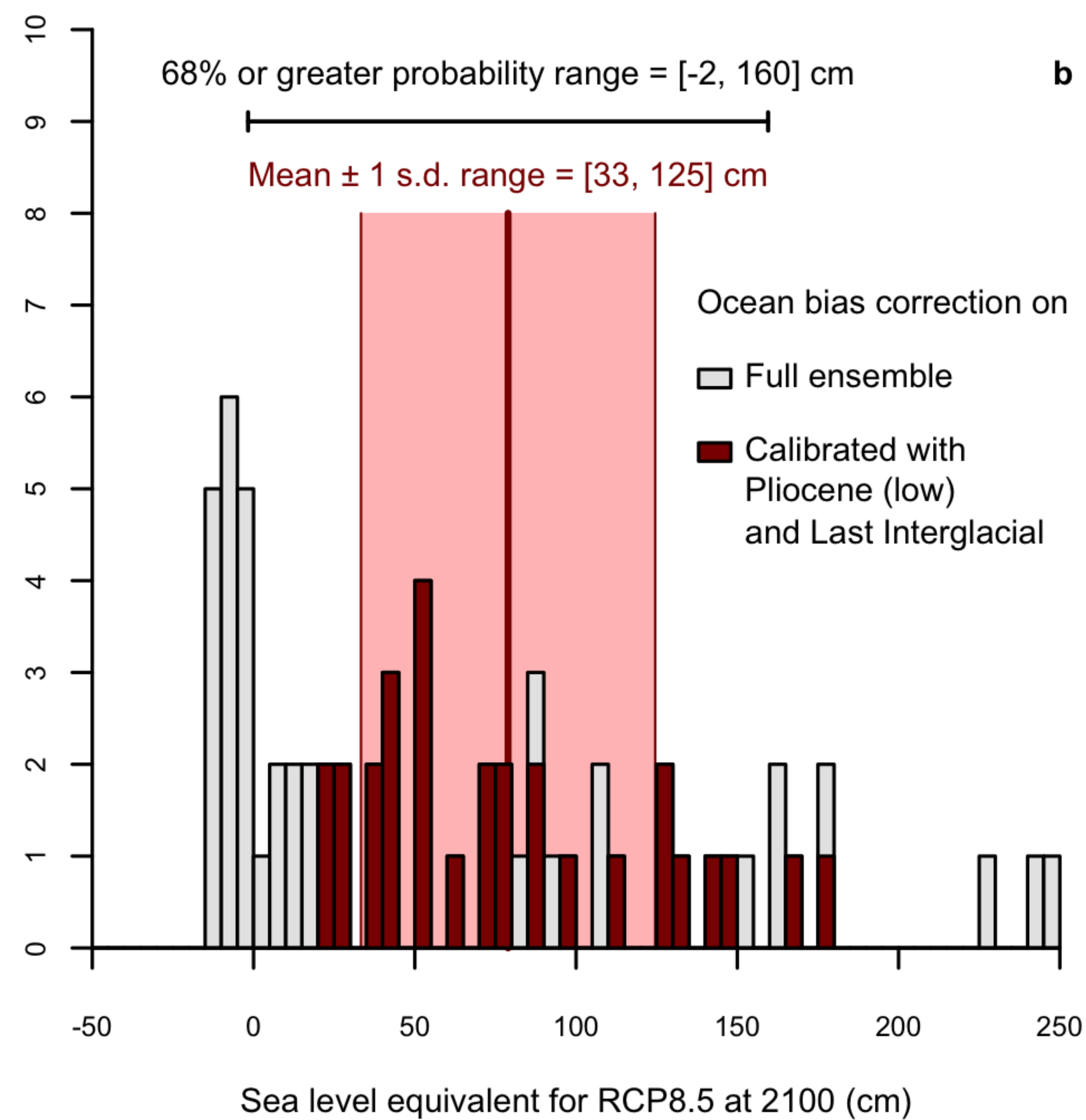
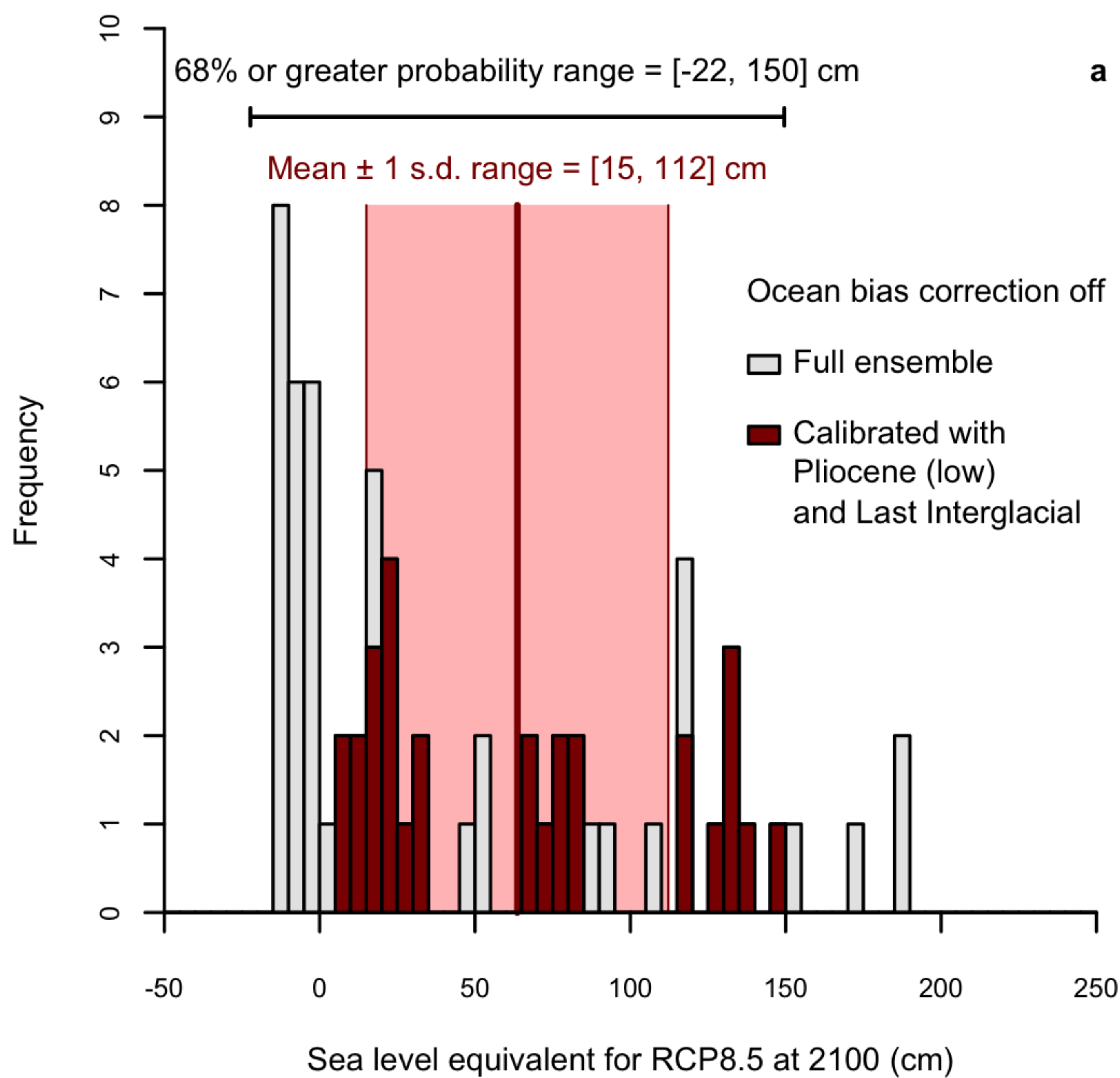
0

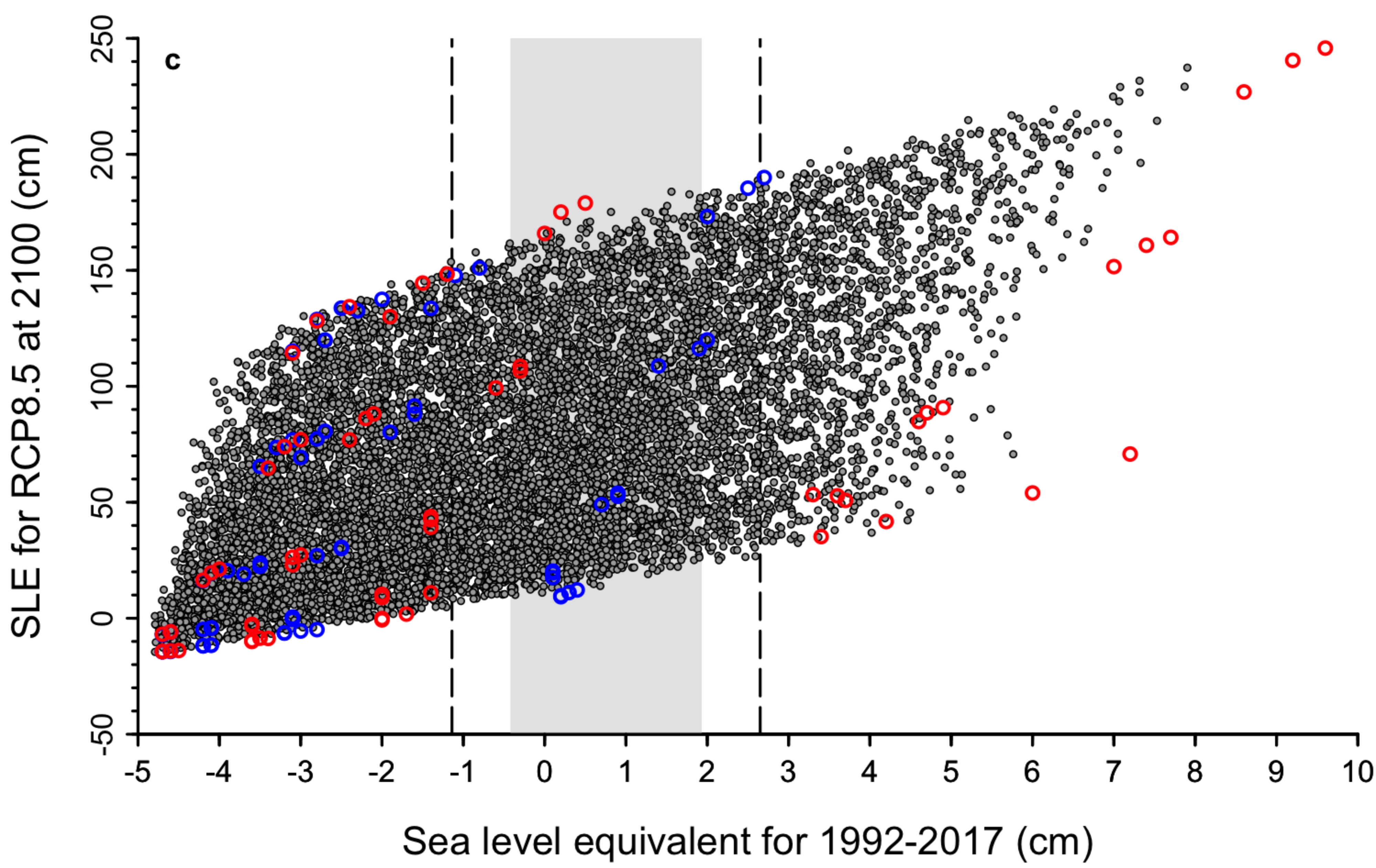
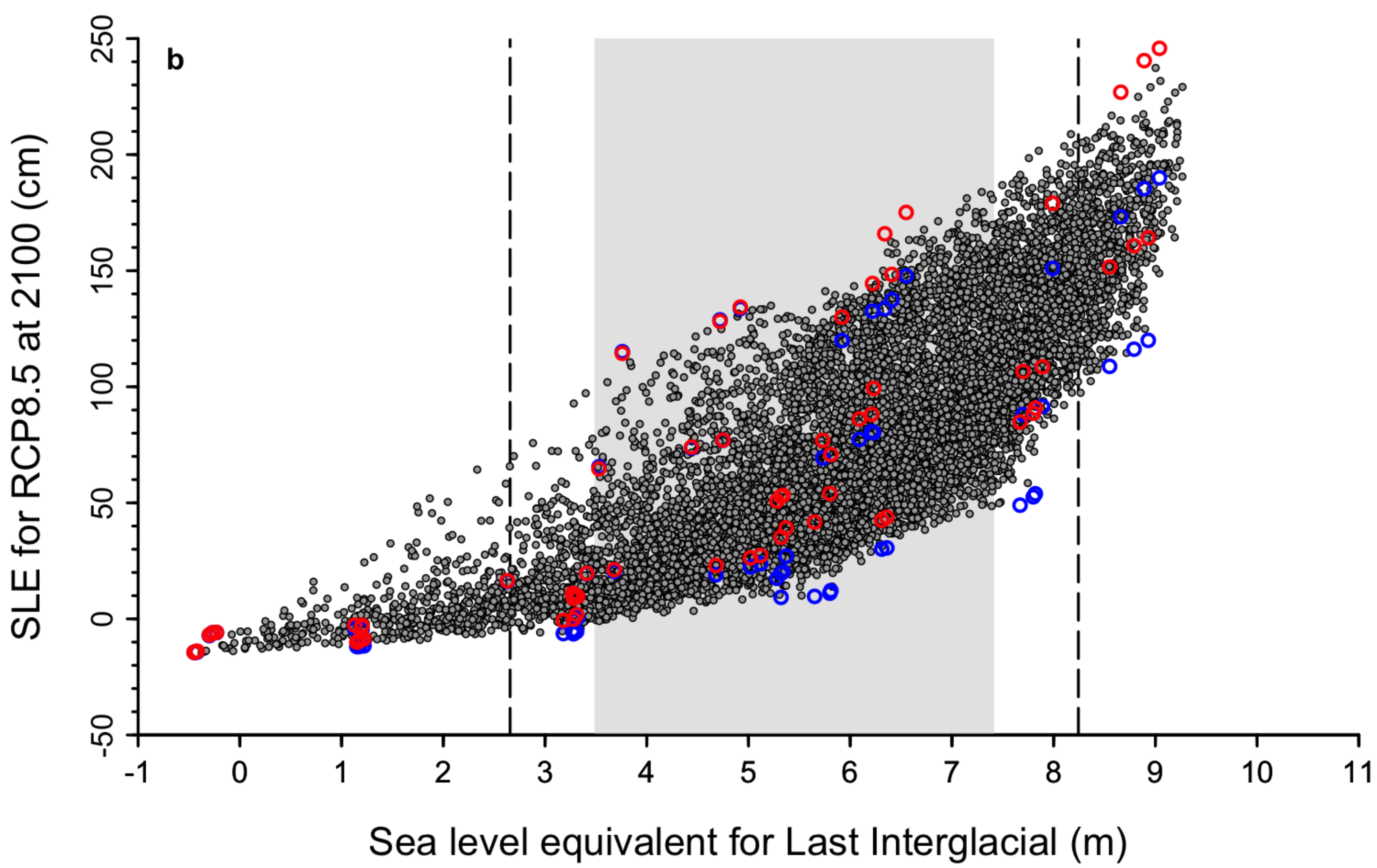
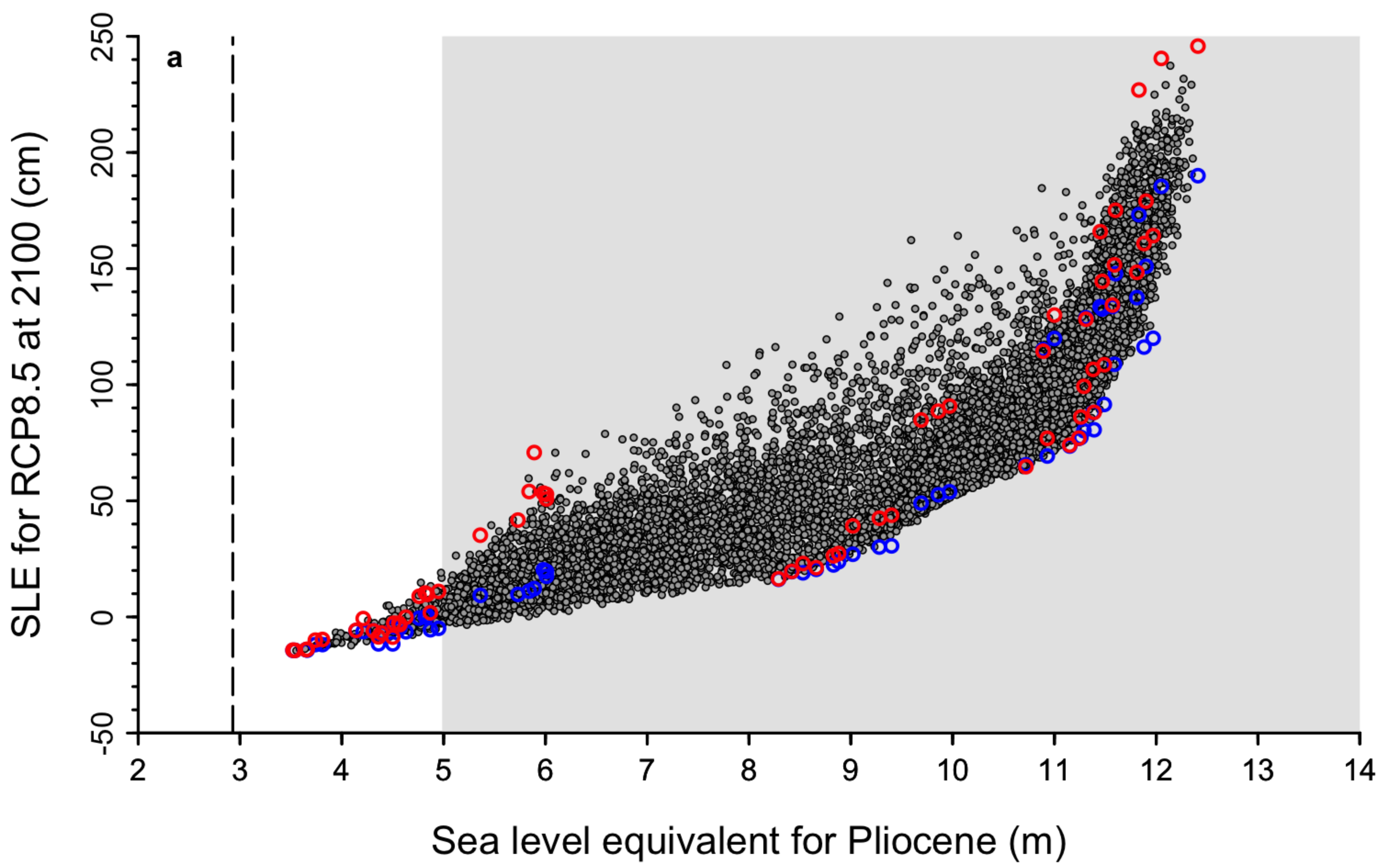
50

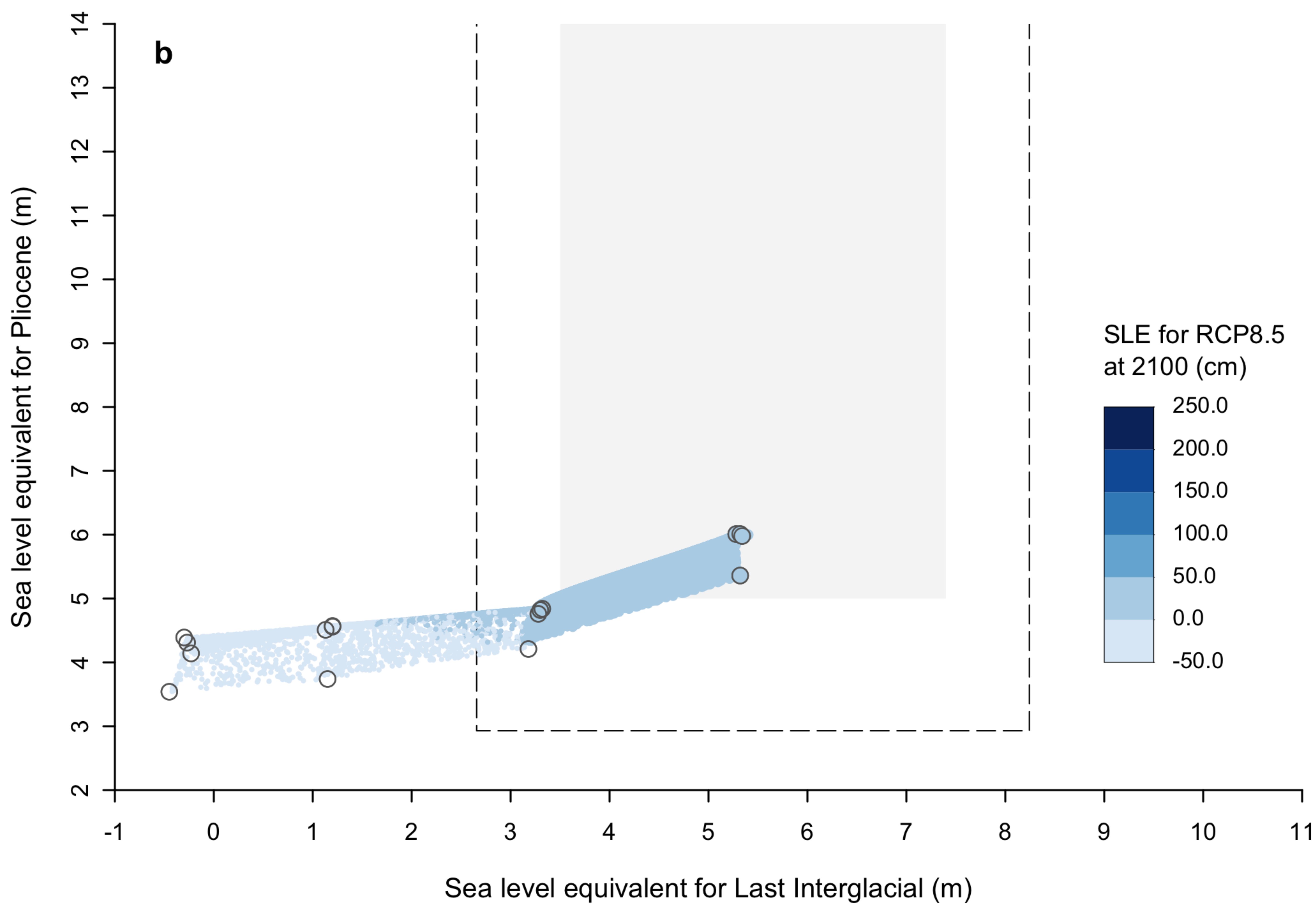
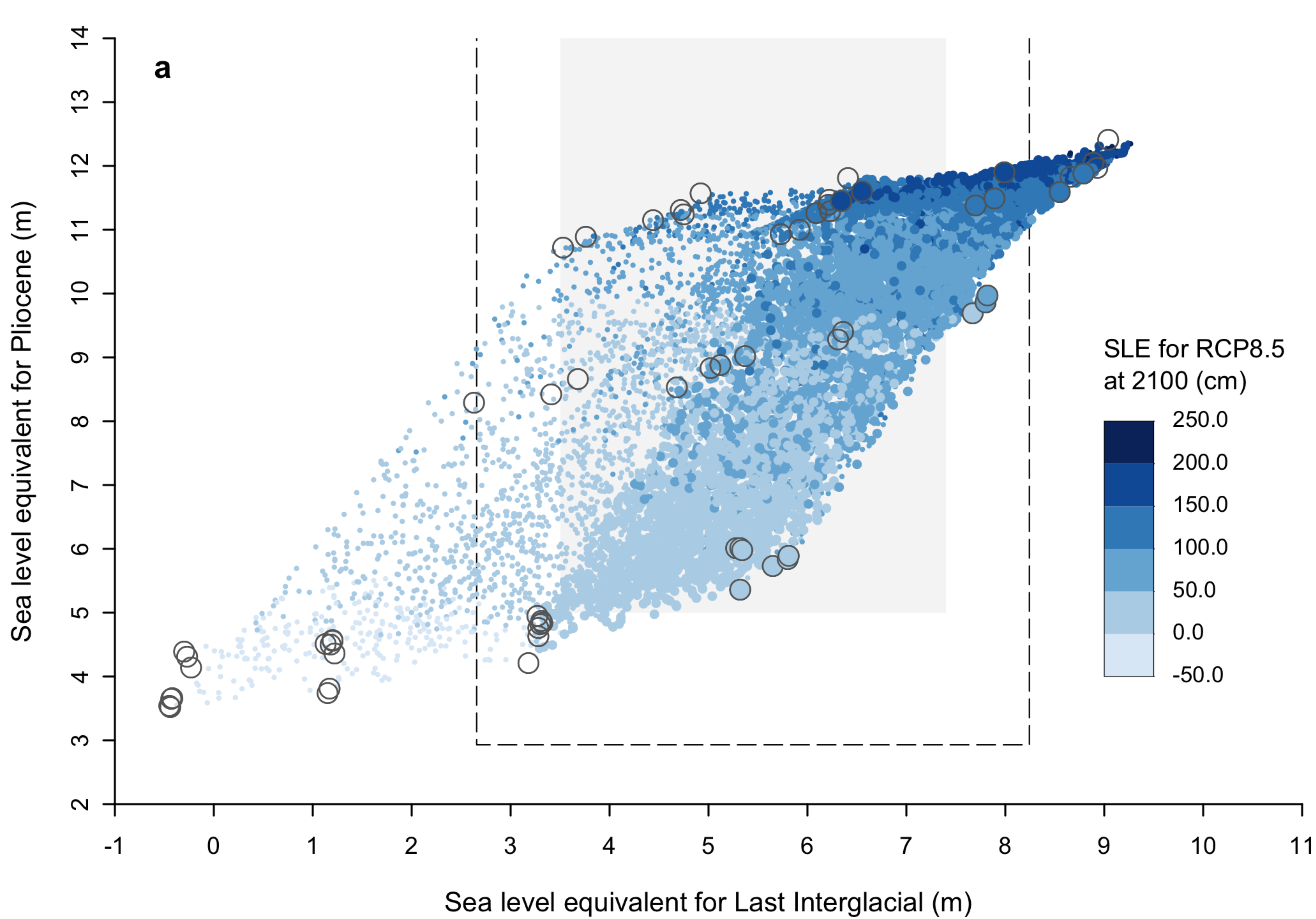
100

150

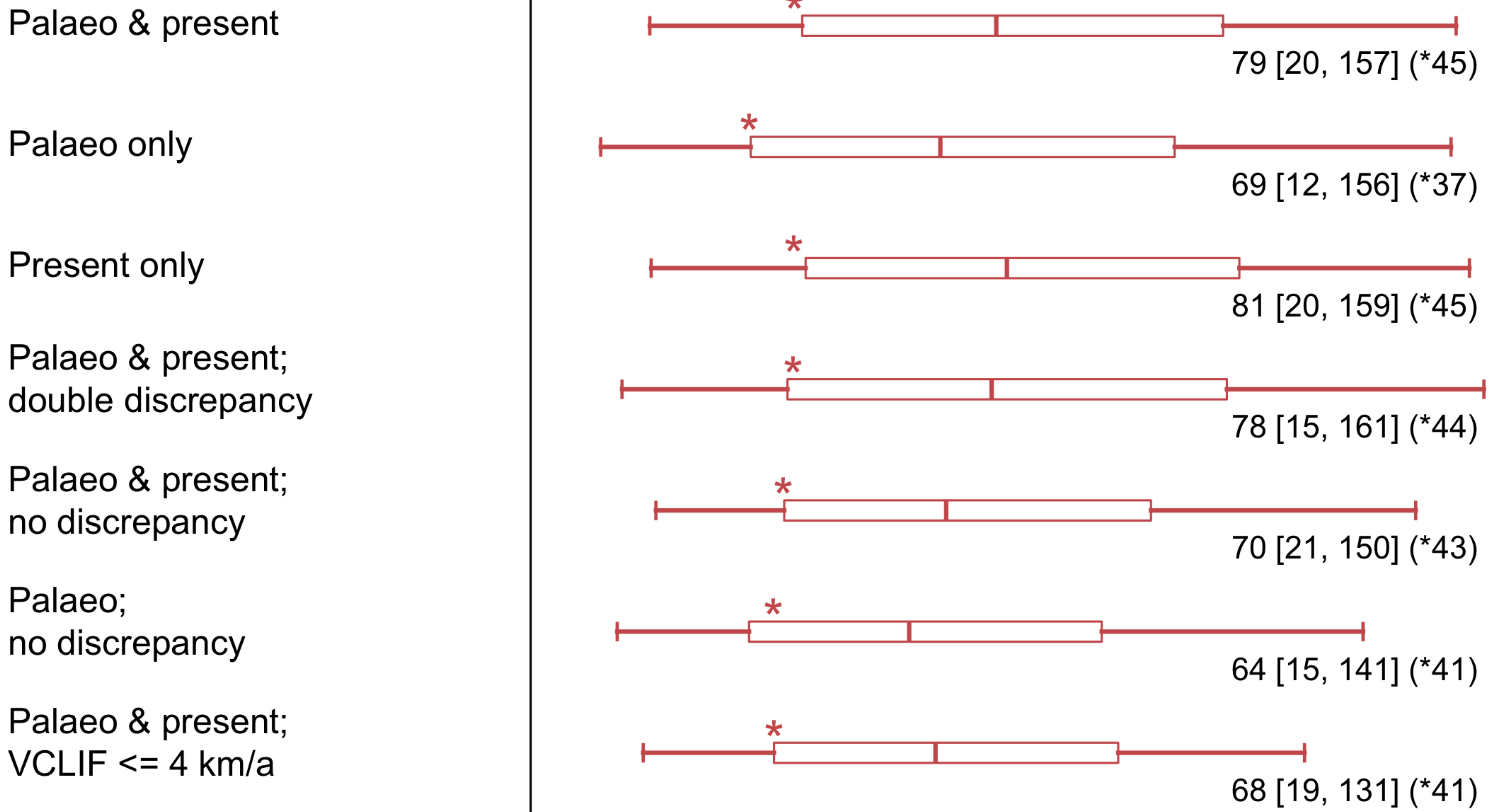




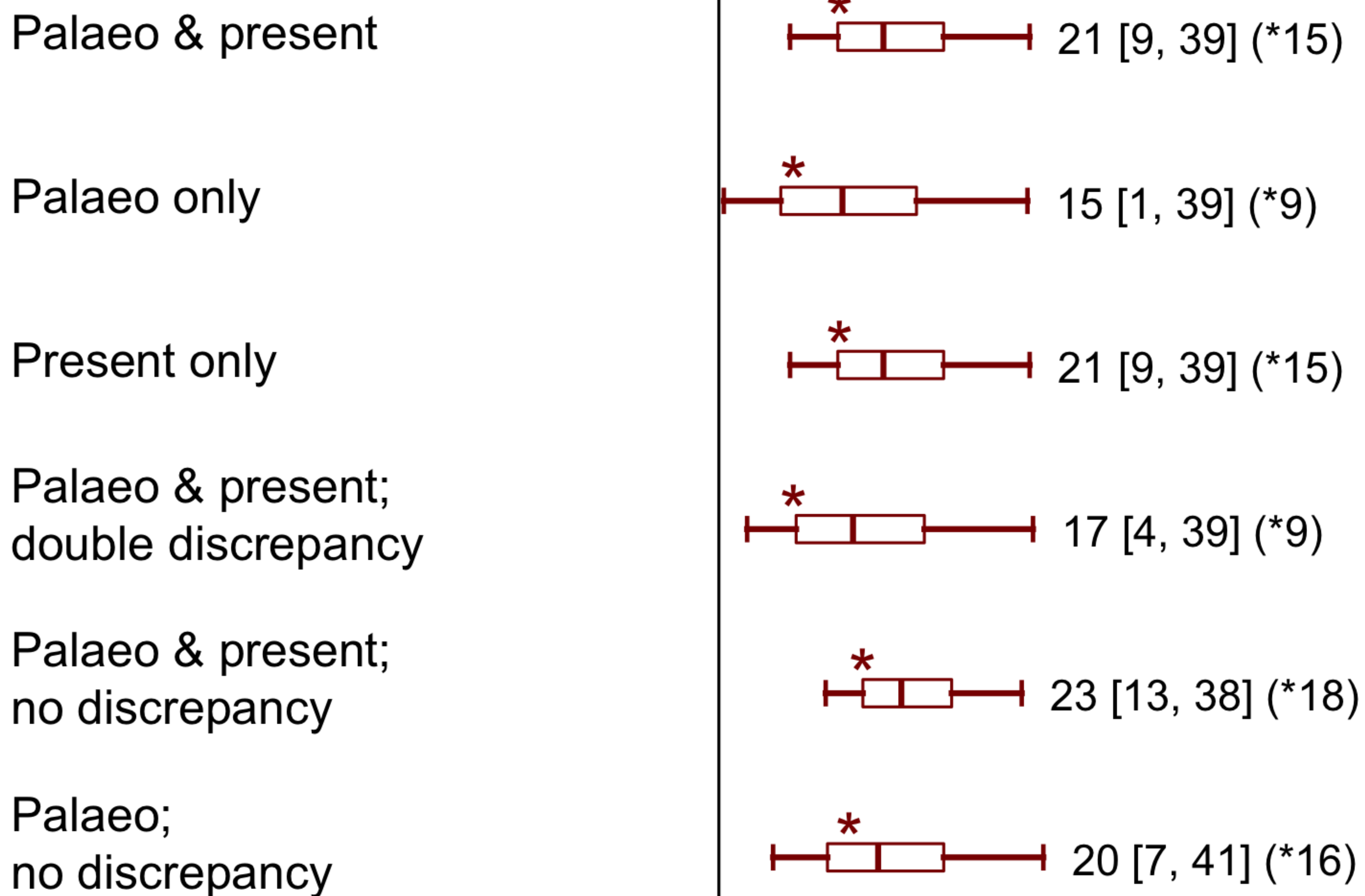




MICI:



No-MICI:



-50

0

50

100

150

Sea level equivalent at 2100 (cm)

